Pion-nucleon scattering in baryon chiral perturbation theory combined with the $1/N_c$ expansion

D. Jayakodige[1,*] and J. L. Goity[1,2,†]

[1]*Department of Physics, Hampton University, Hampton, Virginia 23668, USA*
[2]*Theory Center, Jefferson Lab, Newport News, Virginia 23606, USA*

(Received 11 June 2025; accepted 1 December 2025; published 31 December 2025)

This work implements the combined baryon chiral perturbation theory (BChPT) and $1/N_c$ expansions for pion-nucleon elastic scattering. The effective theory is based on the baryon sector dynamical spin-flavor $SU(4)$ symmetry emergent in the large N_c limit, whose breaking is controlled by the $1/N_c$ expansion. The noncommutativity of the chiral and $1/N_c$ expansions in unitarity corrections (loops) requires a linking of both expansions. As it was shown in the case of baryon masses and currents, the natural linking is the ξ expansion, in which $\mathcal{O}(p) = \mathcal{O}(1/N_c) = \mathcal{O}(\xi)$. The spin-flavor symmetry requires that the ground state baryons span an $SU(4)$ symmetric irreducible representation which implies that in particular N and Δ are active degrees of freedom in the effective theory. The scattering amplitude is expanded to the next-to-next-to leading order in the ξ expansion, corresponding to the one-loop contributions with the leading-order Lagrangian. The results are given for generic N_c in order to demonstrate the consistency of the framework. The spin-flavor symmetry plays a central role in maintaining the consistency of the effective theory with respect to the $1/N_c$ expansion. This consistency manifests itself in an improvement in the convergence of the low energy expansion with respect to the case of the ordinary BChPT without an explicit dynamical Δ, which is known to be inconsistent with the constraints of N_c scaling. Fits to the $\pi N \to \pi N$, S, P, and D partial wave amplitudes from the SAID data base are finally used to test the framework and to determine the energy range of its applicability.

DOI: 10.1103/xbrd-8p5x

I. INTRODUCTION

The formulation of baryon effective theories has spanned different frameworks, starting with the manifestly relativistic baryon chiral perturbation theory (BChPT) [1,2], followed by the same relativistic framework endowed with the infrared regularization scheme [3–5]. Those formulations were implemented with only the spin-1/2 baryons, and later extended to include the spin-3/2 baryons [6]. At the same time, a formulation was developed based on the expansion in $1/m$, m being the baryon mass [7–9], known as the heavy BChPT (HBChPT). Within this framework, and including the spin 3/2 baryons, it was observed that the convergence of the low energy expansion, as shown by the one-loop corrections, is greatly improved due to partial cancellations between the contributions of spin-1/2 and spin-3/2 baryons in loops [8,9]. The poor convergence of the low energy expansion with only spin-1/2 baryons is primarily due to the large πN coupling $g_{\pi NN} \simeq 13.47$. Those observed improvements are the result of a fundamental aspect of QCD, namely the fact that, at sufficiently large N_c, QCD admits an expansion in powers of $1/N_c$ [10]. In the large N_c limit, $g_{\pi NN} = \mathcal{O}(N_c^{3/2})$, while observables such as the πN scattering amplitudes must remain of zeroth order in N_c. This leads to dynamical constraints that must be satisfied at large N_c [11,12]. Those constraints can be associated with an emergent (contracted) spin-flavor symmetry $SU(2N_f)$ in the baryon sector, N_f being the number of light flavors, which in particular requires the inclusion of higher spin baryons, namely the Δ in the physical case $N_c = 3$. In such a framework, the $1/N_c$ expansion can be systematically implemented, providing in particular the deviations from the spin-flavor symmetry as subleading effects in $1/N_c$. The spin-flavor symmetry is already explicit in the Skyrme model [13], and to no surprise it also emerges in the large N_c quark model for baryons, justifying the $SU(4)$ and $SU(6)$ symmetries introduced in the 1960s. Note that the spin-flavor symmetry cannot be realized relativistically, as demonstrated by the Coleman-Mandula theorem [14]. Since at large N_c baryons have masses $\mathcal{O}(N_c)$, and the interest is in studying the low energy limit, where the dynamically relevant momenta and

*Contact author: dulitha@jlab.org
†Contact author: goity@jlab.org

energies are small, the natural reference frame to be used is that in which the baryon has a small 3-momentum, and thus it is almost at rest. Thus, a nonrelativistic framework for baryons is the natural one, where the spin-flavor symmetry can be indeed realized.

Endowing BChPT with the consistency requirements of the large N_c limit is therefore a natural approach. Following on the initial work [15], the implementation of the effective theory at the one-loop level with the corresponding renormalization was initiated [16], where baryon masses and axial currents were studied, followed by studies for three flavors [17]. In the latter references the combined chiral and $1/N_c$ expansions were introduced, in which both expansions are linked according to $\mathcal{O}(p) = \mathcal{O}(1/N_c)$, a scheme coined as the ξ expansion. Such linking is necessary in practice because the different observables contain nonanalytic terms involving their ratios. In particular, for such terms the $1/N_c$ expansion is very slowly convergent as it becomes weighted with respect to the small chiral scales, a feature known as the noncommutativity of the expansions. This framework based on the ξ expansion, hereafter referred to as BChPT $\times$ $1/N_c$, has been applied to masses and currents [16,17]. Further testing is here carried out for the case of π-baryon scattering. As the most studied process in the different versions of effective theory [1,18–29], and empirically as the most accurately known, it is ideal for that purpose.

The first objective of this work is to implement BChPT $\times$ $1/N_c$ at the one-loop level, i.e. up to and including next-to-next-to-leading order (NNLO) in the ξ expansion, for the $\pi B \to \pi B'$ scattering amplitude in the isospin symmetry limit, carrying out the renormalization at generic N_c. The second objective is to confront the results with the $\pi N \to \pi N$ amplitudes as provided by the SAID data base [30,31].

The work is organized as follows: Sec. II presents the BChPT $\times$ $1/N_c$ framework, Sec. III presents the NNLO calculation of the masses and π-baryon couplings, Sec. IV presents the calculation of the π-baryon amplitudes to the NNLO, Sec. V presents the fits to the $\pi N \to \pi N$, S, P, and D partial wave scattering amplitudes from the SAID data base, and Sec. VI presents a summary and conclusions. Finally, the Appendixes contain most of the computational details and explicit results, offering readers adequate information to reproduce the results.

II. BChPT × $1/N_c$

In the large N_c limit, QCD must admit an expansion in powers of $1/N_c$. This is evident at the level of QCD Feynman diagrams as 't Hooft showed 50 years ago [10]. It is expected that the expansion holds at the nonperturbative level, and thus it ought to be implemented at the hadronic level, in particular in effective theories.

The $1/N_c$ expansion requires a proper definition. The one that is most realistic for purposes of phenomenology is 't Hooft's expansion [10], where the number of flavors N_f is kept fixed and quarks are in the fundamental irreducible representation (irrep) of $SU(N_c)$, with the usual Standard Model isospin and the assignments of hypercharges such that, for arbitrary N_c, the SM quantum numbers of the mesons and baryons identified with the physical ones are left unchanged. Since the expansion actually compares different theories, i.e. with different numbers of degrees of freedom, the defining scales of QCD must be prescribed for each N_c. It is convenient to do so with hadronic scales, namely the masses of the ground state mesons, π, K, which are most sensitive to quark masses, and m_ρ for setting the corresponding value of the QCD scale, which along with the quark masses will present subleading $1/N_c$ dependency.

Meson masses scale as $\mathcal{O}(N_c^0)$, while baryon masses are $\mathcal{O}(N_c)$, and the meson decay constants, in particular F_π, are quantities $\mathcal{O}(\sqrt{N_c})$. The meson-meson interactions are suppressed in the large N_c limit with amplitudes scaling as $\mathcal{O}(1/N_c^{n/2})$, where n is the number of initial plus final mesons in the interaction. On the other hand, the meson-baryon couplings can even grow with N_c, as it is the case of the π-baryon coupling $g_{\pi BB}$, which is proportional to $N_c^{3/2}$ [32]. That scaling of $g_{\pi BB}$ and the requirement of a finite π-baryon scattering amplitude in the large N_c limit as required by unitarity, implies the emergence of a dynamical contracted $SU(2N_f)$ spin-flavor symmetry for baryons [11,12,33]. Baryon states must then form multiplets of that symmetry. In particular, for $N_f = 2$, the ground state baryons are in the totally symmetric $SU(4)$ multiplet with $S = I = 1/2, \ldots, N_c/2$ (N_c odd). The states in the multiplet with $S = \mathcal{O}(N_c^0)$ must have mass splitting $\mathcal{O}(1/N_c)$, as required by the aforementioned consistency. The hypothesis that the $1/N_c$ expansion holds down to $N_c = 3$ implies that the nucleon and Δ resonance must belong to the ground state spin-flavor multiplet, and must be active degrees of freedom in the low energy effective theory. Appendix B gives details on $SU(4)$.

The low energy effective theory must be consistent with chiral symmetry and the $1/N_c$ expansion. In the pure Goldstone boson sector this was formulated long ago [34–38], and later it was extended to baryons [15,16,39]. For baryons, the implementation is along the following lines: (i) The active fields in the Lagrangian are the Goldstone bosons and the baryon ground-state spin-flavor multiplet. (ii) The baryon masses being $\mathcal{O}(N_c)$, the $1/N_c$ expansion requires the use of the nonrelativistic baryon fields. (iii) The effective Lagrangians must be manifestly invariant under chiral $SU_L(2) \times SU_R(2)$ as well as under the pertinent continuous and discrete space-time symmetries. (iv) The baryon Lagrangians consist of a composition of a chiral tensor and a spin-flavor tensor built with products of the spin-flavor generators. (v) The spin-flavor tensors must be such that the constraints of the large N_c limit are not violated in observables. The necessary details are provided in the Appendixes, where Appendix A gives

the chiral building blocks, Appendix B gives a summary of the $SU(4)$ algebra and matrix elements in the symmetric $SU(4)$ irrep, and Appendix C gives the bases of spin-flavor tensors of definite spin and isospin, as needed in this work.

The structure of the baryon Lagrangians is therefore of the following general form:

$$\mathcal{L} \sim \mathbf{B}^\dagger T_\chi T_{SF} \mathbf{B}, \tag{1}$$

where $\mathbf{B}$ is the baryon spin-flavor multiplet, T_χ is the chiral tensor formed with the chiral building blocks, and T_{SF} is the spin-flavor tensor which is a composite operator of products of $SU(4)$ generators. Each Lagrangian term is chirally invariant, their chiral order is determined by T_χ, while the leading in $1/N_c$ order is determined by T_{SF}. The Lagrangian will contain leading and subleading orders in $1/N_c$, the latter from the expansion of the chiral tensor through the factors of $1/F_\pi$ multiplying the pion fields. The spin-flavor tensors are defined to contain the $1/N_c$ suppression factor determined by the n-bodyness of the tensor, in this way the low energy constant (LEC) in front of each Lagrangian term is $\mathcal{O}(N_c^0)$, followed by subleading corrections. This in particular implies the obvious fact that fully determining the effective theory for arbitrary N_c requires explicit knowledge of QCD at different N_c, which could be achieved using lattice QCD. This is however no significant hindrance to the applications to the real world with $N_c = 3$.

The low energy effective theory contains two small scales, namely the small energy/momenta characteristic of the chiral expansion and the $\mathcal{O}(1/N_c)$ baryon mass splittings, e.g. $\Delta = m_\Delta - m_N$. Observables contain dependencies on ratios of both scales, e.g. M_π/Δ, which preclude the independent low energy and $1/N_c$ expansions. Such dependencies appear in the loop contributions involving Goldstone Boson and baryon propagators. This "noncommutativity" of the expansions demands that either only one of them is implemented, or they be linked. The latter is evidently the option that works best for the real world as it was shown in several works [16,17], in which the ξ-power-counting scheme was introduced, according to which $\mathcal{O}(p) = \mathcal{O}(1/N_c) = \mathcal{O}(\xi)$. Indeed, nonanalytic terms stemming from loop corrections or pole terms in amplitudes that involve ratios of the form $p/(1/N_c)$ are slowly convergent in either expansion, and need to be kept at face value. Lagrangians are, therefore, organized by their order in the ξ expansion, and as shown later, the ultraviolet (UV) divergencies of loop contributions to observables are analytic in ξ, and respect N_c power consistency.

While the baryon Lagrangians needed for this work are given in Appendix D, it is convenient to present here the LO one, that provides the interactions for the one-loop calculations:

$$\mathcal{L}_B^{(1)} = \mathbf{B}^\dagger \left(iD_0 + \mathring{g}_A u^{ia} G^{ia} - \frac{C_{HF}}{N_c}\hat{S}^2 + \frac{c_1 N_c}{2\Lambda}\langle \chi_+ \rangle \right) \mathbf{B}, \tag{2}$$

which is expressed in terms of the chiral building blocks in Appendix A. The first term contains the residual energy of the baryon in the heavy mass expansion and two-pion vertices (Weinberg-Tomozawa terms). The second term gives the single pion coupling to the baryons in addition to the axial current coupling. The third term gives the residual mass contribution to the baryon according to its spin, giving mass splittings $\mathcal{O}(1/N_c)$ between baryons with spin $\mathcal{O}(N_c^0)$. The final term gives the LO quark mass contribution to the baryon mass, and also two-pion vertices. The arbitrary scale Λ is introduced for convenience to have c_1 dimensionless, as well as in the higher order Lagrangians to have dimensionless LECs, and will be set equal to m_ρ in the explicit calculations. The axial coupling $\mathring{g}_A$ is at LO related to the axial coupling g_A of the nucleon at $N_c = 3$ by $\frac{5}{6}\mathring{g}_A = g_A = 1.267$. For notational convenience, the mass shift operator is defined by $\delta\hat{m} = \frac{C_{HF}}{N_c}\hat{S}^2$, where the spin-flavor singlet contribution from the quark masses is omitted, since only baryon mass differences appear in loop diagrams. Appendix D (Table V) gives the vertices from $\mathcal{L}_B^{(1)}$ needed in this work.

The NLO and NNLO calculations involve the one-loop diagrams. Their power counting is defined by the resulting terms analytic in chiral and $1/N_c$ powers, the ξ power being the sum of them. In general, individual diagrams containing vertices proportional to $\mathring{g}_A$ will give contributions that violate large N_c consistency. Such terms must then be canceled when adding all the pertinent diagrams. These cancellations provide, in particular, useful checks of the calculations.

III. BARYON MASSES AND AXIAL COUPLINGS

A. Masses

At LO the baryon mass formula is simply

$$m_B(S) = m_0 + \frac{C_{\rm HF}}{N_c} S(S+1) - 2c_1 N_c \frac{M_\pi^2}{\Lambda}, \tag{3}$$

where m_0 is the common mass $\mathcal{O}(N_c)$, $C_{\rm HF}$ is determined from the $\Delta - N$ mass difference, and c_1 gives the LO dependence on M_π, which is proportional to N_c. In the ξ expansion this term is the LO contribution to the σ term, which is therefore a quantity $\mathcal{O}(N_c)$, implying that even at large N_c a finite fraction of the baryon mass is due to the current quark masses.

At NNLO the masses include the one-loop terms shown in Fig. 1 and counterterms (CT).

FIG. 1. One-loop contributions to the baryon self-energy.

The one-loop contribution to the self-energy operator reads

$$\hat{\Sigma}(p^0) = i\left(\left(\frac{\mathring{g}_A}{F_\pi}\right)^2 \sum_n G^{ia}\mathcal{P}_n G^{ia}\mathcal{I}(\delta m_n - p^0, M_\pi) + 2N_c c_1 \frac{M_\pi^2}{\Lambda F_\pi^2}\mathcal{I}(M_\pi)\right), \tag{4}$$

where $\mathcal{P}_n$ is the projector onto the nth component of the spin-flavor baryon multiplet, and

$$\begin{aligned}
\mathcal{I}(Q, M_\pi) &= \frac{1}{d-1}\int \widetilde{d^d k}\frac{\vec{k}^2}{(k^0 - Q + i\epsilon)(k^2 - M_\pi^2 + i\epsilon)} \\
&= \frac{i}{3(4\pi)^2}\left(Q\left((3M_\pi^2 - 2Q^2)\left(\lambda_\epsilon - \log\frac{M_\pi^2}{\mu^2}\right) + 7M_\pi^2 - \frac{16}{3}Q^2\right)\right. \\
&\quad \left. + 4(M_\pi^2 - Q^2 - i\epsilon)^{3/2}\left(\frac{\pi}{2} - \arctan\frac{Q}{\sqrt{M_\pi^2 - Q^2 - i\epsilon}}\right)\right) \\
\mathcal{I}(M_\pi) &= \int \widetilde{d^d k}\frac{1}{k^2 - M_\pi^2 + i\epsilon} = \frac{i}{(4\pi)^2}M_\pi^2\left(\lambda_\epsilon + 1 - \log\frac{M_\pi^2}{\mu^2}\right),
\end{aligned} \tag{5}$$

where $d = 4 - 2\epsilon$, $\widetilde{d^d k} = \frac{d^d k}{(2\pi)^d}$ and $\lambda_\epsilon \equiv \frac{1}{\epsilon} - \gamma_E + \log 4\pi$. These loop integrals and others needed in this work are presented in detail in Appendix E.

The contribution to the wave function renormalization factor is given by

$$\delta Z(p^0) = -\frac{\partial}{\partial p^0}\Sigma(p^0). \tag{6}$$

For a particular baryon state n, the one-loop contribution to the mass and the wave function renormalization is evaluated by replacing $p^0 \to \delta m_n$. With this, the UV divergent pieces can be expressed as spin-flavor operators for the mass shift and wave function renormalization, namely,

$$\begin{aligned}
\Sigma^{\rm UV} &= -\frac{\lambda_\epsilon}{(4\pi)^2}\left(\left(\frac{\mathring{g}_A}{F_\pi}\right)^2\left(M_\pi^2 G^{ia}[\delta\hat{m}, G^{ia}] - \frac{2}{3}G^{ia}[\delta\hat{m}, [\delta\hat{m}, [\delta\hat{m}, G^{ia}]]]\right) + 2c_1\frac{N_c M_\pi^4}{F_\pi^2\Lambda}\right) \\
&= \frac{\lambda_\epsilon}{(4\pi)^2}\left(\left(\frac{\mathring{g}_A}{F_\pi}\right)^2\frac{C_{\rm HF}}{N_c}\left(M_\pi^2\left(-\frac{3}{8}N_c(N_c+4) + \frac{5}{2}\hat{S}^2\right)\right.\right. \\
&\quad \left.\left. + \frac{1}{3}\left(\frac{C_{\rm HF}}{N_c}\right)^2\left(3N_c(N_c+4) + (5N_c(N_c+4) - 24)\hat{S}^2 - 28\hat{S}^4\right)\right) + 2c_1\frac{N_c M_\pi^4}{F_\pi^2\Lambda}\right) \\
\delta Z^{\rm UV} &= -\frac{\lambda_\epsilon}{(4\pi)^2}\left(\frac{\mathring{g}_A}{F_\pi}\right)^2(M_\pi^2\hat{G}^2 - 2G^{ia}[\delta\hat{m}, [\delta\hat{m}, G^{ia}]]) \\
&= \frac{\lambda_\epsilon}{(4\pi)^2}\left(\frac{\mathring{g}_A}{F_\pi}\right)^2\left(\frac{1}{16}M_\pi^2(-3N_c(N_c+4) + 8\hat{S}^2)\right. \\
&\quad \left. + \frac{1}{2}\left(\frac{C_{\rm HF}}{N_c}\right)^2(3N_c(N_c+4) + 2(N_c(N_c+4) - 12)\hat{S}^2 - 8\hat{S}^4)\right).
\end{aligned} \tag{7}$$

Note that the UV divergent piece of the mass is $\mathcal{O}(N_c^0)$ and driven by the mass splitting term. On the other hand the nonanalytic contributions to the mass are $\mathcal{O}(N_c)$. In the large N_c limit, the wave function renormalization correction is proportional to $\mathcal{O}(N_c) \times M_\pi^2$: this indicates that approaching the large N_c limit with a baryon effective theory based on perturbation theory is not consistent. This is one additional argument in favor of the linked ξ expansion.

The baryon mass differences remain as $\mathcal{O}(1/N_c)$, and for $N_c = 3$ one obtains:

$$m_\Delta - m_N = C_{\rm HF} + \left(\frac{\mathring{g}_A}{F_\pi}\right)^2 \frac{1}{(4\pi)^2}\left(\frac{1}{6}C_{\rm HF}\left(5(3M_\pi^2 - 2C_{\rm HF}^2)\left(\lambda_\epsilon - \log\frac{M_\pi^2}{\mu^2}\right) + 35M_\pi^2 - \frac{80C_{\rm HF}^2}{3}\right)\right.$$
$$\left. + (M_\pi^2 - C_{\rm HF}^2 - i\epsilon)^{3/2}\left(\pi - \frac{10}{3}\arctan\frac{C_{\rm HF}}{\sqrt{M_\pi^2 - C_{\rm HF}^2 - i\epsilon}}\right)\right) + \text{CT}, \tag{8}$$

where CT indicates the mass counterterms.

B. Axial and $\pi BB'$ couplings

At LO the axial vector current matrix elements and pion-baryon interactions are given by

$$\langle B'|A^{ia}|B\rangle = \mathring{g}_A\langle B'|G^{ia}|B\rangle,$$
$$\langle B'|\mathcal{L}_B^{(1)}|\pi^a(k)B\rangle = -i\frac{\mathring{g}_A}{F_\pi}k^i\langle B'|G^{ia}|B\rangle, \tag{9}$$

satisfying the Goldberger-Treiman relation.

The NNLO one-loop contributions are shown in Fig. 2. The analysis of the axial currents was presented in Ref. [16]. The $\pi BB'$ vertex to one-loop order is given by

$$i\Gamma^a(k,p,p') = \frac{\mathring{g}_A}{F_\pi}k^i\left(G^{ia} + i\left(\frac{\mathring{g}_A}{F_\pi}\right)^2\sum_{n,n'}\int\widetilde{d^dk'}\frac{G^{jb}\mathcal{P}_{n'}G^{ia}\mathcal{P}_nG^{lb}k'^jk'^l}{(k'^2 - M_\pi^2)(p^0 - k'^0 - \delta m_n)(p'^0 - k'^0 - \delta m_{n'})}\right.$$
$$\left. - \frac{1}{2}\{\delta Z, G^{ia}\} - \frac{1}{3}\frac{1}{F_\pi^2}G^{ia}\mathcal{I}(M_\pi) + \text{CTs}\right),$$
$$= \frac{\mathring{g}_A}{F_\pi}k^i\left(G^{ia} - i\left(\frac{\mathring{g}_A}{F_\pi}\right)^2\sum_{n,n'}G^{jb}\mathcal{P}_{n'}G^{ia}\mathcal{P}_nG^{jb}\frac{\mathcal{I}(\delta m_n - p^0, M_\pi) - \mathcal{I}(\delta m_{n'} - p'^0, M_\pi)}{p^0 - p'^0 - \delta m_n + \delta m_{n'}}\right.$$
$$\left. - \frac{1}{2}\{\delta Z, G^{ia}\} - \frac{1}{3}\frac{1}{F_\pi^2}G^{ia}\mathcal{I}(M_\pi) + \text{CTs}\right), \tag{10}$$

where the term involving the wave function renormalization correction is key to restoring the N_c consistency, cancelling contributions $\mathcal{O}(N_c^{3/2})$ from the first diagram (a).

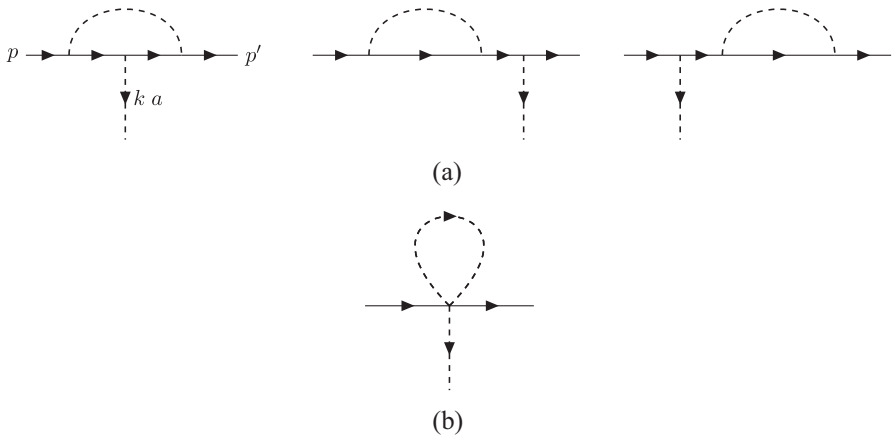

FIG. 2. One-loop diagrams for the pion-baryon interaction. Diagrams (a) and (b) are respectively proportional to $\mathring{g}_A^3$ and $\mathring{g}_A$.

For baryon momenta on-shell, i.e. setting $p^0 = \delta m_{\rm in}$, $p'^0 = \delta m_{\rm out}$, the UV divergence can be given in the operator form:

$$i\Gamma^a_{\rm UV} = -\frac{\lambda_\epsilon}{(4\pi)^2}\frac{\mathring{g}_A}{F_\pi}k^i\left(-\frac{M_\pi^2}{F_\pi^2}G^{ia} + \frac{1}{6}\left(\frac{\mathring{g}_A}{F_\pi}\right)^2\left(\left(2\left(\frac{C_{\rm HF}}{N_c}\right)^2(N_c(N_c+4)-2) - 3M_\pi^2\right)G^{ia} + 10\left(\frac{C_{\rm HF}}{N_c}\right)^2(\{\hat{S}^2, G^{ia}\} - (N_c+2)S^iI^a)\right)\right). \tag{11}$$

The UV divergent pieces illustrate the two most important facts about the higher order corrections to the pion-baryon couplings: (i) the quark mass contributions are suppressed as $\mathcal{O}(1/N_c)$ with respect to the LO and do not affect the spin-flavor structure of the LO, and (ii) the terms that affect the spin-flavor structure, i.e. terms proportional to S^iI^a, are corrections of $\mathcal{O}(1/N_c^2)$ with respect to the LO. Finally, the Goldberger-Treiman discrepancy remains, as it is well known, an effect that is only the result of a CT. For the CT Lagrangian see Appendix D, Eq. (D10). The LECs cannot be fixed completely as at $N_c = 3$ the only experimentally accessible couplings are $g_{\pi NN}$, $g_{\pi N\Delta}$, and the g_A of the nucleon. In the present analysis the $\pi N \to \pi N$ amplitudes will be used to determine them.

IV. SCATTERING AMPLITUDES

This section presents the formalism for the general case of $\pi B \to \pi B'$ scattering. It is presented for general N_c for the purpose of identifying the order in N_c of the different contributions. A rigorous implementation of renormalization at the NNLO is carried out.

The contributions to the scattering amplitude are decomposed into those with baryon pole singularities and those without, as depicted in Fig. 3. In the one-loop diagrams, this decomposition is performed as explained in Appendix F.

A. LO scattering amplitude

The LO T-matrix, given by the diagrams in Fig. 4 and expressed as an operator in spin-flavor reads

$$iT^{ba}_{LO} = -i\left(\frac{\mathring{g}_A}{F_\pi}\right)^2 k_1^i k_2^j \sum_n \left(\frac{G^{jb}\mathcal{P}_n G^{ia}}{p_1^0 + k_1^0 - \delta m_n + i\epsilon} + \frac{G^{ia}\mathcal{P}_n G^{jb}}{p_1^0 - k_2^0 - \delta m_n + i\epsilon}\right) + \frac{1}{F_\pi^2}\left(-2ic_1 N_c \frac{M_\pi^2}{\Lambda}\delta^{ab} + \frac{1}{2}(k_1^0 + k_2^0)\epsilon^{abc}I^c\right). \tag{12}$$

This amplitude is precisely the one that requires the emergence of spin-flavor symmetry [33], since the individual terms proportional to $\mathring{g}_A^2$ have contributions $\mathcal{O}(N_c)$,

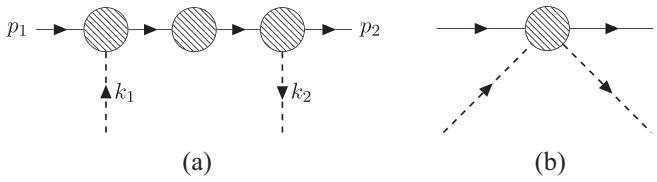

FIG. 3. General decomposition of the scattering amplitude into pole (a) and no-pole (b) contributions. To diagram (a) the crossed diagram must be added.

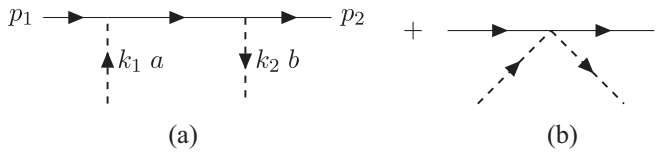

FIG. 4. LO contributions to the scattering amplitude. To diagram (a) the crossed diagram must be added. Diagrams (a) and (b) are respectively proportional to $\mathring{g}_A^2$ and $\mathring{g}_A^0$.

and such contributions must cancel when the terms are added. Moreover, the pole terms reflect the noncommutative nature of the chiral and $1/N_c$ expansions. The LO pole terms will combine with the higher order ones to yield the result shown in Eq. (15).

B. One-loop corrections to the πB scattering amplitude

The scattering amplitudes at NLO and NNLO involve the one-loop diagrams of Figs. 5–7 and the CT contributions from Lagrangians equations (D5)–(D8), which provide for the renormalization. The loops are organized in three groups according to their power in $\mathring{g}_A$.

For one- and two-particle reducible diagrams, the decomposition into pole and no-pole terms is carried out following Eqs. (F1) and (F2). The results for the individual diagrams, including details on the UV divergencies, are presented in Appendix F. The spin-flavor tensors in the diagrams are projected in t-channel (J, I), where $J, I = 0, 1, 2$. Since the ground state baryon spin-flavor multiplet consists only of states $S = I$, only transitions with baryon $\Delta S = 0, 1, 2$ can occur. In the physical case $N_c = 3$,

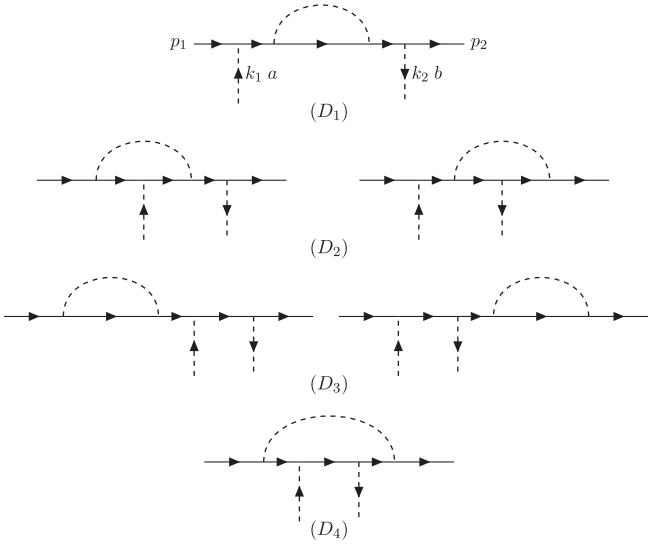

FIG. 5. Diagrams proportional to $\mathring{g}_A^4$.

$\Delta S = 0,\ 1$. The CT Lagrangians for renormalizing the no-pole contributions are then constructed following those t-channel projections, using the basis of spin-flavor operators in Appendix C, Table IV. Those Lagrangians contain terms $\mathcal{O}(\xi^2$ and $\xi^3)$. Throughout, in the construction of the higher order Lagrangians the LO equations of motion are used, namely,

$$\begin{aligned} iD_0\mathbf{B} &= \left(\frac{C_{\rm HF}}{N_c} - c_1\frac{N_c}{2\Lambda}\langle\chi_+\rangle - \mathring{g}_A u^{ia}G^{ia}\right)\mathbf{B} \\ D_\mu u^\mu &= \frac{i}{2}\chi_-, \end{aligned} \tag{13}$$

along with the identities:

$$\begin{aligned} D_\mu u_\nu - D_\nu u_\mu &= -f_{-\mu\nu} \\ [D_\mu, D_\nu] &= -i\Gamma_{\mu\nu} \\ \Gamma_{\mu\nu} &= \frac{1}{2}f_{+\mu\nu} + \frac{1}{4}[u_\mu, u_\nu]. \end{aligned} \tag{14}$$

For each of the sets of diagrams, the sum of the no-pole UV divergent parts is decomposed into t-channel (J, I) and, for general N_c, the corresponding spin-flavor tensors are expressed in terms of the basis in Table IV. In the set proportional to $\mathring{g}_A^4$, individual diagrams are $\mathcal{O}(N_c^2)$, thus two orders must exactly cancel in the sum of the UV divergent pieces, which is indeed the case as shown in the result Eqs. (F11)–(F12). Similarly, the set proportional to $\mathring{g}_A^2$, where diagrams $D_{6,7,8}$ vanish identically, has diagrams $\mathcal{O}(N_c)$, with such contributions cancelling in the sum of the UV divergent pieces, as shown by Eq. (F31). Finally, the diagrams proportional to $\mathring{g}_A^0$ are individually $\mathcal{O}(N_c^0)$, and have the property that they involve only a fixed spin baryon state throughout the diagrams.

In the CT Lagrangians, the LECs are expressed in the form $X = \beta_X\frac{\lambda\epsilon}{(4\pi)^2} + X(\mu)$, where $X(\mu)$ is the renormalized LEC at the scale μ, and the β function β_X is adjusted to eliminate the corresponding UV divergence in the $\overline{\rm MS}$ subtraction scheme. The β functions are shown in Table VII. Note that the one-loop amplitudes' UV divergencies show both NLO and NNLO terms, which in general appear together in a given set of diagrams. For this reason, the results are given for the complete one-loop amplitudes, with no attempt at separating NLO from NNLO, although this can be performed in a rigorous way. Such a separation must also include the nonanalytic contributions, a task that is somewhat lengthy, and therefore it is not presented in the results.

There are several interesting observations to be made, namely:

(i) The T-matrix UV divergencies proportional to $\mathring{g}_A^4$ have no M_π dependencies.

(ii) The UV divergencies contain different orders in ξ, as shown in Eqs. (F11), (F31), and (F39).

(iii) In all cases the renormalization scale μ appears in the single combination $\log\frac{M_\pi^2}{\mu^2}$.

(iv) All nonanalytic terms involving the residual masses of the baryons, i.e., δm_n, appear in combination with the pion mass in factors of the form $(\delta m_n - \delta m_{n'})^\nu \log\frac{M_\pi^2}{\mu^2}$ $(\nu = 1,\ 3)$, $(M_\pi^2 - (\delta m_n - \delta m_{n'})^2)^{\nu/2}$ $(\nu = 1,\ 3)$, $\arctan\frac{(\delta m_n - \delta m_{n'})}{\sqrt{M_\pi^2 - (\delta m_n - \delta m_{n'})^2}}$.

(v) The evaluations of the matrix elements of the spin-flavor tensors for the nonanalytic contributions, which involve projections on different baryon intermediate states, are performed explicitly using the results for the different matrix elements of the $SU(4)$ generators in Eq. (B2), as the results cannot be reduced to simple expressions in terms of the basis spin-flavor tensors.

Adding the pole terms from the leading-order amplitude, Eq. (12), together with the higher-order pole contributions from the diagrams D_1, D_2, D_3, and D_5, and after performing the mass and pion-baryon coupling renormalizations, results in the following general form of the pole amplitude:

$$\begin{aligned} \langle B'|iT^{ba}_{\rm pole}|B\rangle = -i\frac{k_1^i k_2^j}{F_\pi^2}\sum_n \mathring{g}_{ABB_n}\mathring{g}_{AB_nB'} \\ \times\left(\frac{\langle B'|G^{jb}\mathcal{P}_n G^{ia}|B\rangle}{p_B^0 + k_1^0 - \delta m_n^R + \frac{i}{2}\Gamma_n} \right. \\ \left. + \text{crossed}^*\right), \end{aligned} \tag{15}$$

where $\mathring{g}_{ABB'}$ is the renormalized coupling, which at LO is equal to $\mathring{g}_A$, δm_n^R is the renormalized residual mass,

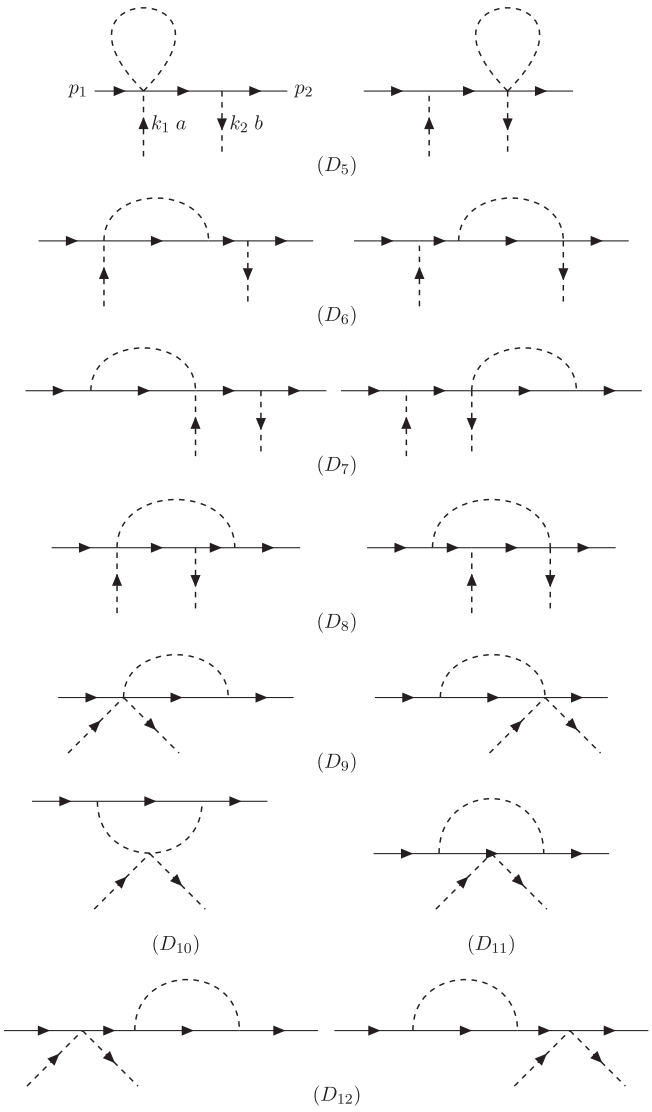

FIG. 6. Diagrams proportional to $\mathring{g}_A^2$. Diagrams $D_{6,7,8}$ vanish identically. Tadpole diagrams, which only renormalize the baryon mass, are not shown.

$p_B^0 = \delta m_B^R + \frac{\vec{k}_1^2}{2m_0}$ is the residual energy of the external baryon that includes the kinetic energy $\mathcal{O}(\xi^3)$, and $\Gamma_n = \mathcal{O}(\xi^2)$ is the decay width. Such terms must be included at the NNLO of the calculation.[1] For the crossed diagram, the star indicates that Γ_n must be set to vanish when the self-energy in the B_n baryon propagator in the u-channel is real. This in particular holds if $B = N$, which is the case of main interest here. At $N_c = 3$, only Γ_Δ is needed and reads

$$\Gamma_\Delta = \frac{\mathring{g}_{AN\Delta}^2 m_N}{6\pi(16F_\pi)^2 m_\Delta^4}\lambda_K(m_\Delta^2, m_N^2, M_\pi^2)^{3/2}, \tag{16}$$

[1]The renormalized self-energy of the baryon is here approximated by its residual mass and decay width, *a la* Breit-Wigner, which is an excellent approximation in the present context.

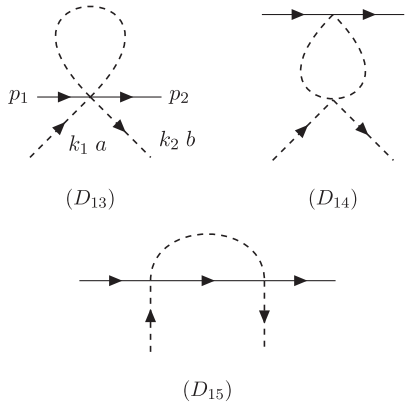

FIG. 7. Diagrams proportional to $\mathring{g}_A^0$.

where λ_K is the Källen phase space function. Because of the P-wave nature of the decay, in order to be accurate enough, the exact phase space factor must be used.

V. $\pi N \to \pi N$ SCATTERING AND FIT TO DATA

This section aims at testing the effective theory by fitting to the $\pi N \to \pi N$ data, for which the SAID data base [30,31] is used.

The T-matrix is expressed in the standard center-of-mass (CM) t-channel decomposition in terms of the spin-nonflip $g^\pm$ and spin-flip $h^\pm$ amplitudes:

$$T^{ba}_{\pi N\to\pi N} = \frac{E_N + m_N}{2m_N}(\delta^{ab}(g^+(s,t) - i(\vec{k}_1\times\vec{k}_2)\cdot\vec{\sigma}h^+(s,t)) + i\epsilon^{bac}\tau^c(g^-(s,t) - i(\vec{k}_1\times\vec{k}_2)\cdot\vec{\sigma}h^-(s,t))), \tag{17}$$

giving the s-channel partial wave amplitudes,

$$f^\pm_{\ell\pm}(s) = \frac{E_N + m_N}{16\pi\sqrt{s}}\int_{-1}^{1} dz(g^\pm(s,t(z))P_\ell(z)) + k^2 h^\pm(s,t(z))(P_{\ell\pm1}(z) - zP_\ell(z)), \tag{18}$$

where $t(z) = -2k^2(1-z)$, k is the CM momentum, and $z = \cos\theta$, θ being the CM scattering angle. The projection to s-channel isospin is given by the well-known relation:

$$\begin{pmatrix} f^{1/2}_{\ell\pm} \\ f^{3/2}_{\ell\pm}\end{pmatrix} = \begin{pmatrix} 1 & 2 \\ 1 & -1\end{pmatrix}\begin{pmatrix} f^+_{\ell\pm} \\ f^-_{\ell\pm}\end{pmatrix}. \tag{19}$$

Throughout the exact kinematics for E_N, s and t are used.

For a generic partial wave amplitude the corresponding phase shift is defined by

$$f(s) = -\frac{i}{2k}(e^{2i\delta(s)}\eta(s) - 1), \tag{20}$$

with the inelasticity factor $0 \le \eta(s) \le 1$. In the present case, where the analysis is carried out below the onset of the second resonance region, it turns out that one can approximate $\eta \sim 1$

throughout [30,31]. Unitarity is only approximate in the effective theory, and only $\mathrm{Re}f(s)$ is affected by the NLO and NNLO LECs to be fitted, while $\mathrm{Im}\,f(s)$ is entirely determined by the LO Lagrangian, and is thus less accurate than the real part. It is therefore more realistic to fit to the real part of the partial wave amplitudes and then use Eq. (20) to give the imaginary part through the obtained phase shift.

At LO, the contributions arise from three sources: the Weinberg–Tomozawa term, the c_1 term driven by the quark masses, which contribute only to the S-wave amplitudes, and the pole terms proportional to $\mathring{g}_A^2$ that contribute only to the P-wave amplitudes. A realistic description of the Δ pole at LO requires including its decay width, so the LO amplitudes are fully determined by just four parameters: $c_1, C_{HF}, \mathring{g}_A$, and Γ_Δ. At this order, only S- and P-wave amplitudes are present: the S-waves should determine c_1, while the P-waves determine the remaining parameters. As is well known, the LO alone gives a poor description, as depicted in Figs. 8 and 9.

The LO fit to the S-waves shows that c_1 is very sensitive to the range of energy included in the fit and to the constraint from the scattering length a_0^+. Fitting the S-waves in the range $k < 150$ MeV, without the scattering length constraint gives $c_1/\Lambda \sim 0.14/m_\rho$, which is unrealistic as it corresponds to a negative σ term. On the other hand, the scattering length a_0^+ gives $c_1/\Lambda = (-0.047 \pm 0.017)/m_\rho$, which gives an unrealistically small σ term. The values of a_0^+ and the σ term require the inclusion of NLO and NNLO contributions for consistency, with the counterterm proportional to the LEC $\alpha_{00}^{(3)}$ in Eq. (F45) playing a crucial role. Note that the LO description of the S_{11} amplitude fails above $k \sim 100$ MeV, while for the S_{31} fails above $k \sim 250$ MeV.

The fit to the P waves is dominated by the P_{33} one, giving $C_{HF} = 260$ MeV, $\mathring{g}_A = 1.67$, and $\Gamma_\Delta = 80$ MeV. The value of $\mathring{g}_A$ corresponds to a nucleon's axial coupling $g_A = 1.39$, to be compared with the physical one $g_A = 1.267$. The other P-waves receive contributions as follows: P_{11} from the direct diagram with nucleon pole and from the crossed one, while P_{13} and P_{31} receive contributions only from the crossed one. The LO P_{11} amplitude and phase shift disagrees with the data at rather low pion momentum, $k > 50$ MeV, which is a well known fact [21], and therefore the higher order contributions must be very important in this case, providing crucial structure absent at LO. The LO P_{13} and P_{31} have a wider range of agreement and the higher order contributions are thus of relative smaller magnitude than in the case of the P_{11}.

At NLO and NNLO, the various one-loop diagrams contribute as follows:

(i) Diagrams proportional to $\mathring{g}_A^4$ affect only the P-waves.
(ii) Diagrams proportional to $\mathring{g}_A^2$ contribute to the S-waves, except for diagram D_{10}, which also contributes to P- and D-waves.
(iii) Diagrams proportional to $\mathring{g}_A^0$ contribute to the S-waves, with D_{14} also contributing to P-waves, and to the D_{33} and D_{35} waves.
(iv) The D-waves originate solely from the one-loop diagrams $D_{10,14}$ and are UV finite.

Only a subset of the NLO and NNLO LECs in the CT Lagrangians can be determined by $\pi N \to \pi N$ scattering. Those are shown by the CT contributions to the T-matrix in Eq. (F45). Since subleading M_π dependencies of the amplitudes are not explicitly known, and the subleading in $1/N_c$ dependencies of the LECs require explicit knowledge at $N_c > 3$, some LECs appear in combinations that the fit can determine, namely, $\overline{c}_1 \equiv c_1 - \frac{1}{2N_c}(\alpha_{00}^{(1)} + \frac{N_c M_\pi^2}{\Lambda^2}\alpha_{00}^{(2)})$ and $\bar{\alpha}_{00}^{(3)} \equiv \alpha_{00}^{(3)} + N_c \frac{M_\pi^2}{\Lambda^2}\alpha_{00}^{(4)}$.

The fits up to NNLO to the SAID single-energy solutions were performed in different ranges of pion CM momentum k, up to a maximum of 350 MeV, which corresponds to $\sqrt{s} = 1.38$ GeV. In the fits, the scale Λ used to render the LECs dimensionless is taken to be m_ρ. The S-wave scattering lengths as determined from pionic atoms [40–42] are taken as inputs, where the values given in the latter reference are used. The real parts of the amplitudes up to and including D-waves along with the imaginary part of the P_{33} amplitude are fitted. The latter presents an imaginary part that, in the case of the pole contribution involves the NNLO couplings and masses, is thus accurate to the NNLO, and ought to be included in the fit. The results of the fit up to $k = 350$ MeV along with the phase shifts are shown in Figs. 8 and 9. Depicted are the imaginary parts obtained via unitarization from the real parts, as well as the imaginary parts that result from the perturbative calculation, which in general are less accurately described for the reason mentioned earlier. The results shown here do not separate between NLO and NNLO, an exercise that can be carried out, as pointed out earlier, with some significant effort in order to determine how the expansion behaves.

In the range $k \leq 350$ MeV, the inelasticity factor is taken to be unity for all partial waves, as it can be confirmed by the SAID analysis [30,31]. In particular this requires for the P_{33} partial wave that $k \times \mathrm{Re}f_{1+}^3$ reaches a maximum value $+1/2$ and a minimum value $-1/2$ around the Δ resonance, which is fulfilled by the fit within the estimated error band. The no-pole terms from the nonanalytic and CT contributions are essential for restoring consistency with the unitarity constraint on $\mathrm{Re}f_{1+}^3$ Eq. (20). The errors of S- and P-wave data are in general much smaller than the expected theoretical error of the NNLO calculations. The rather large χ^2 per degree of freedom of the fits is indicative of that disparity. Fitting the S waves up to $k = 250$ MeV and the P and D waves up to $k = 350$ MeV results in $\chi^2_{\mathrm{dof}} \sim 60$. This is however very dependent on the convergence range in k for the different partial waves. An estimate of the NNNLO effects is thus an elaborate task which will not be pursued here. Instead, an error band for the theoretical amplitudes is estimated by fitting 500 bootstrap resamplings of the data for each partial wave. The error band corresponds to the 95% confidence interval and provides a visual representation

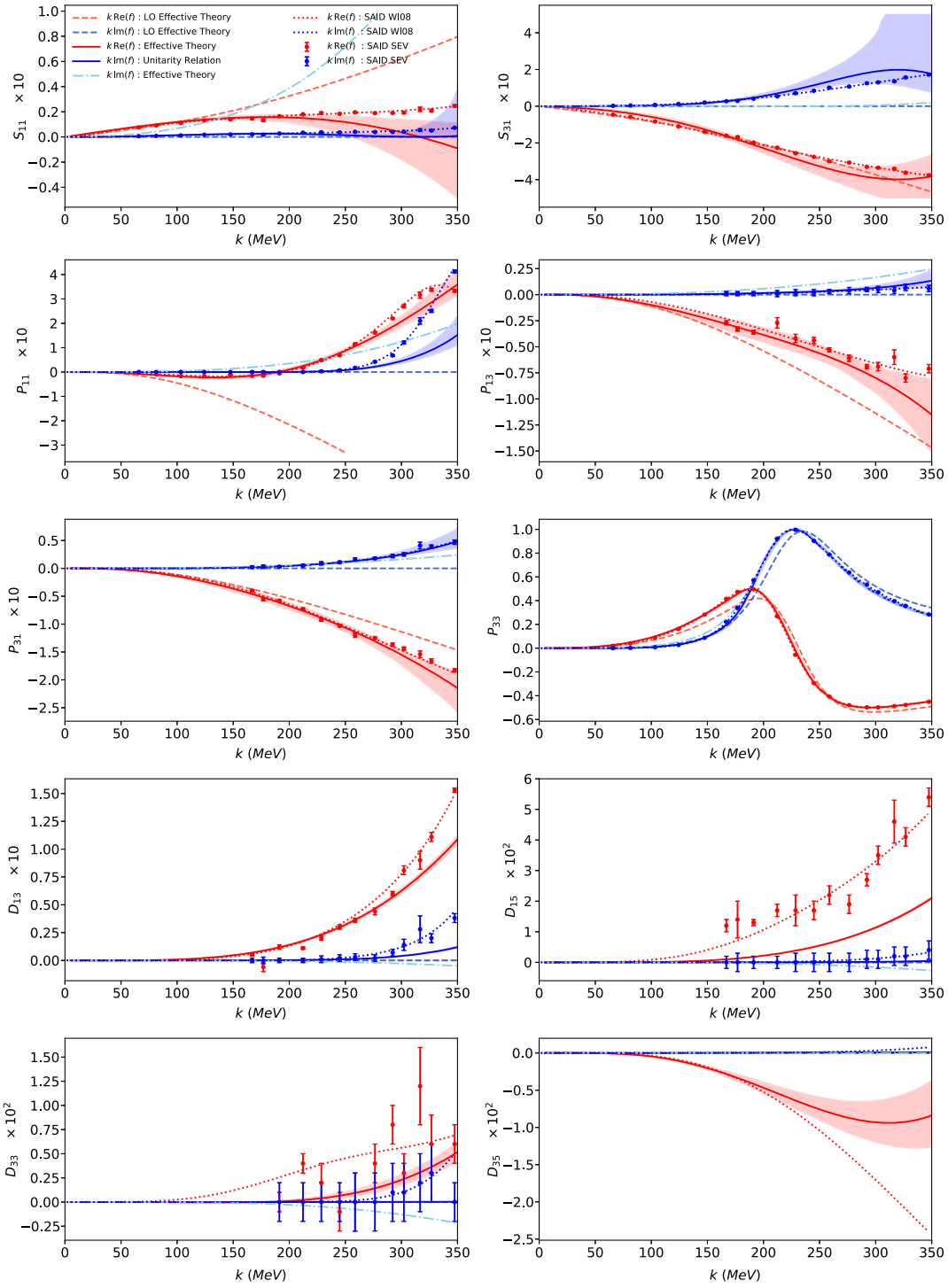

FIG. 8. Fits to the partial wave amplitudes Ref and the Im f of the P_{33} partial wave. Plots show $k \times \mathrm{Re}f$ (solid red) and $k \times \mathrm{Im}\, f$ vs k from phase shift as determined from Ref using the unitarity-relation equation (20) (solid blue), and from absorptive parts of one-loop diagrams (dash-dot light blue). The error band estimates are obtained by bootstrap resampling the data. The data is from the SAID database [30,31]: WI08 solution (dotted), and the data points, used for the fits, are the single energy solution SEV. The LO fit results are depicted by the dashed curves.

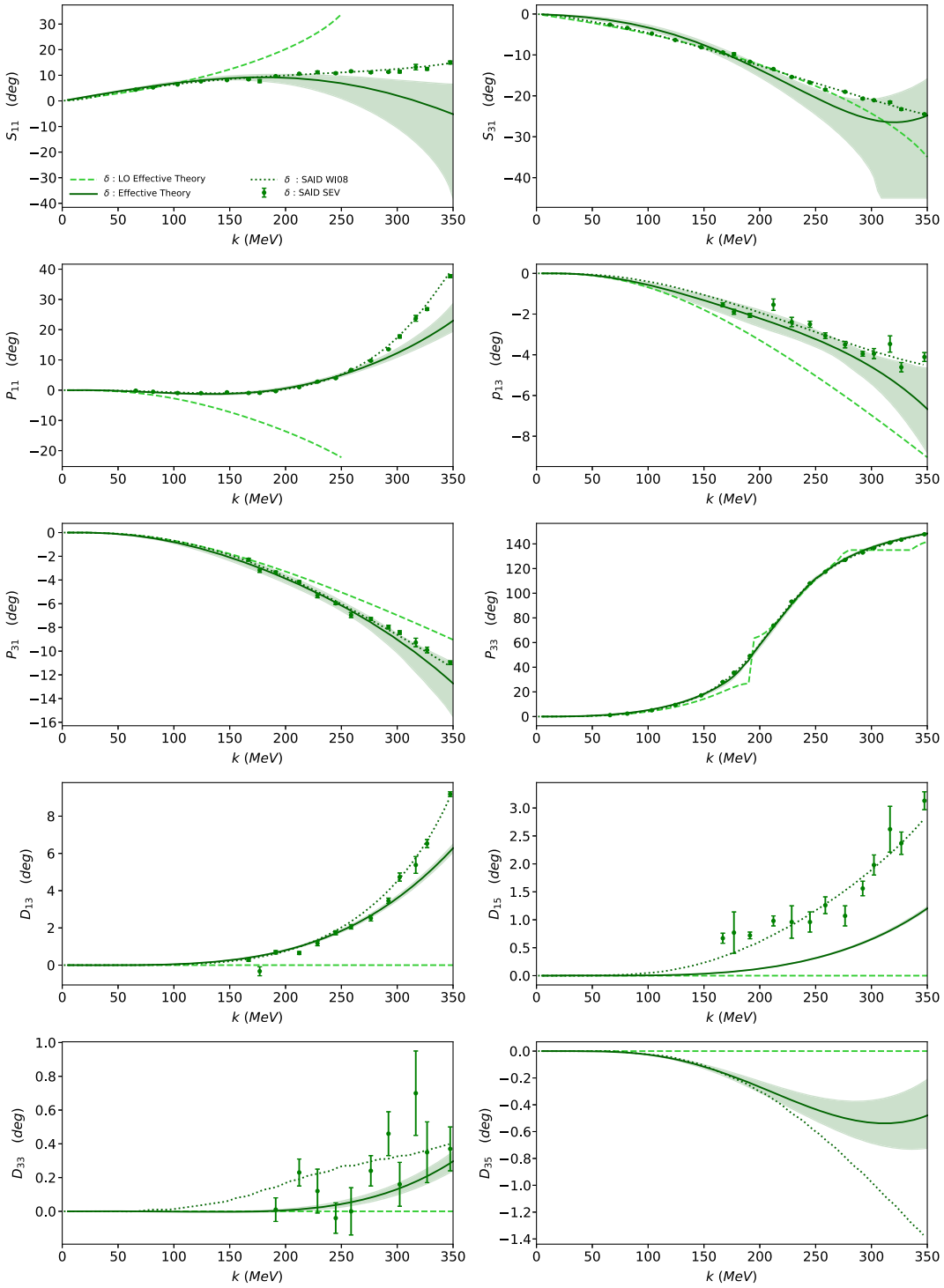

FIG. 9. Phase shifts: SAID WI08 solution (dotted), data points from SEV solution, and from the fit up to NNLO in Fig. 8 using the unitarity relation equation (20) (solid). The LO phase shifts, obtained from the unitarity relation, are depicted by the dashed curves.

of the theoretical uncertainty. The parameters resulting from those fits are shown in Table I.

As mentioned earlier, at LO there is a disparity between fixing the a_0^+ scattering length and the value of the σ term. The CT proportional to $\bar{\alpha}_{00}^{(3)}$, that only contributes to a_0^+ and vanishes at the Cheng-Dashen point, is crucial in resolving the disparity. The fit determines the combination of LECs $\bar{c}_1$, which gives now a rather large tree-level contribution to

the σ term (at the chosen renormalization scale), about 140 MeV. A full-fledged analysis of the σ term will be presented elsewhere [43].

The analysis of the partial wave amplitudes gives strong support for the implementation of the $1/N_c$ consistency conditions in the framework of BChPT $\times$ $1/N_c$ using the ξ expansion. A key observation is the range of validity of the expansion: at NNLO, the approach yields a consistent description of the amplitudes for CM pion momenta up to 200–350 MeV, depending on the specific partial wave.

The real parts of the amplitudes are described by the effective theory within different ranges of CM pion momentum, namely, the S- and P-waves are described up to about 250 MeV, while in particular the P_{33} wave is well described up to 350 MeV. The D-waves are more challenging due to their naturally small magnitudes as they vanish at LO and have only finite one-loop and no CT contributions. Among the D-wave channels, the D_{13} and D_{35} are consistent with expectations, while those for D_{33} and D_{15} exhibit discrepancies that merit further investigation. It is certain that the NNNLO implementation is necessary for a realistic description of the D-waves.

The result for the coupling $\mathring{g}_{ANN}$, disregarding the Goldberger-Treiman discrepancy, implies a determination of the nucleon axial coupling $g_A = 1.325$, and the result for the $\mathring{g}_{AN\Delta}$ coupling gives $\Gamma_\Delta = 134$ MeV, which is about 10% larger than the fitted value. Note that the fitted value agrees well with the Breit-Wigner width's estimate from the Particle Data Group (PDG) [44].

The fit result for $C_{\rm HF}$ is similar to the LO one if one takes for the Δ mass the Breit-Wigner PDG value. On the other hand, the value for $\mathring{g}_A$ resulting from the NNLO fit to the scattering amplitudes is smaller than the LO $\mathring{g}_A = 1.52$ and the NNLO $\mathring{g}_A = 1.45$ from the BChPT $\times$ $1/N_c$ analysis [16] of the nucleon's axial coupling. The S-wave scattering lengths were constrained to lie within the experimental uncertainties, yielding $a_0^+ = 0.006/M_\pi$ and $a_0^- = 0.087/M_\pi$, in good agreement with the experimental values [42], $a_0^+ = (0.0078 \pm 0.0028)/M_\pi$ and $a_0^- = (0.0866 \pm 0.0010)/M_\pi$.

As shown in Fig. 8, the one-loop results significantly improve upon the LO predictions for the real parts of the partial wave amplitudes, while also including the missing absorptive contributions and D-wave components. The range of agreement between the bootstrapped error bands and the data defines the range of applicability of the effective theory, and the natural sizes of the fitted LECs further validate its consistency in the present context. A comparison with previous BChPT analyses that include explicit Δ degrees of freedom [21,24,25,29] indicates that the BChPT $\times$ $1/N_c$ framework achieves a comparable, and in some cases even broader, energy range of agreement with the experimental phase shifts. To be more specific, Appendix G presents the comparison, shown in Table VIII. It is noted that, because the frameworks of those works are not equivalent to the present one, it is possible that there is a difference in number of LECs involved in the fits.

TABLE I. Low energy constants from fit. The combinations of LECs $\bar{c}_1$ and $\bar{\alpha}_{00}^{(3)}$ are defined in the text. The range for the fit parameters in brackets indicates their standard deviation obtained via bootstrap resampling, and should not be confused with actual uncertainty. The results correspond to $\Lambda = \mu = m_\rho$.

$C_{\rm HF}$ [MeV]	304.3 (0.8)	$\bar{\alpha}_{00}^{(3)}$	−4.43(0.27)
Γ_Δ [MeV]	119.7 (1.4)	$\alpha_{00}^{(5)}$	0.35 (0.31)
$\mathring{g}_A$	1.18	$\alpha_{01}^{(1)}$	3.90 (1.29)
$\bar{c}_1$	−0.90(0.05)	$\alpha_{01}^{(2)}$	−1.99(0.81)
g_{ANN}	1.58 (0.03)	$\alpha_{01}^{(3)}$	0.81 (0.20)
$g_{AN\Delta}$	1.81 (0.01)	$\alpha_{01}^{(4)}$	−0.49(0.27)
		$\alpha_{10}^{(1)}$	2.60 (0.57)
		$\alpha_{11}^{(1)}$	−6.17(0.74)
		$\alpha_{11}^{(2)}$	4.28 (1.96)

VI. SUMMARY AND CONCLUSIONS

This work implements the combined framework of BChPT and the $1/N_c$ expansion for low-energy pion-baryon scattering up to NNLO in the ξ expansion. This approach respects both the constraints of chiral symmetry and the systematic expansion in $1/N_c$ derived from QCD. The ξ expansion retains, without further expansion, nonanalytic terms where the chiral and $1/N_c$ expansions are not simultaneously valid—terms that typically exhibit slow convergence in either expansion performed individually. This treatment is essential for realistic descriptions of QCD in the physical world. The role of the $SU(4)$ spin-flavor symmetry is central to ensuring manifest consistency with the large-N_c limit of observables. In particular, it leads to a suppression of loop corrections via cancellations among diagrams that would otherwise violate large-N_c scaling.

A test of the framework with elastic πN scattering shows a natural range of applicability for pion CM momentum up to about 250 MeV, and larger for the P_{33} channel up to 350 MeV. The range of S-waves is primarily limited by the contributions from the diagrams proportional to $\mathring{g}_A^0$, which only involve the nucleons throughout, and are therefore the same as in the case of the ordinary BChPT with only active nucleons. While the real parts of the partial wave amplitudes are well described in significant part due to the available NLO and NNLO LECs, departures from unitarity are manifested in the imaginary parts, in particular in the S-waves above pion momentum 200–250 MeV. Those departures happen in

amplitudes where those absorptive parts are very small. These results motivate further investigations using BChPT $\times 1/N_c$ in the context of low-energy scattering [43], particularly focusing on the extraction of the πN sigma term and a comprehensive analysis that incorporates currents and a more detailed study of πN scattering.

ACKNOWLEDGMENTS

This material is based upon work supported by the U.S. Department of Energy, Office of Science, Office of Nuclear Physics under Contract No. DE-AC05-06OR23177 (J. L. G.), and by the National Science Foundation, Grant No. PHY 1913562 (J. L. G., D. J.). The authors are indebted to Christian Weiss for discussions and to Ron Workman and Igor Strakovsky for clarifications on the pion-nucleon SAID database.

DATA AVAILABILITY

The data that support the findings of this article are not publicly available. The data are available from the authors upon reasonable request.

APPENDIX A: CHIRAL BUILDING BLOCKS

Using standard notations, the building blocks needed for constructing chiral tensors are

$$\begin{aligned}
&\Pi(x)=\pi^a(x)\tau^a\\
&u(x)=e^{i\frac{\Pi(x)}{2F_\pi}}\ U(x)\equiv u^2(x)\\
&\ell_\mu=v_\mu-a_\mu r_\mu=v_\mu+a_\mu\\
&\Gamma_\mu=-\Gamma_\mu^\dagger=\frac{i}{2}(u^\dagger(\partial_\mu-i(v_\mu+a_\mu))u+u(\partial_\mu-i(v_\mu-a_\mu))u^\dagger)\\
&D_\mu=\partial_\mu-i\Gamma_\mu\\
&u_\mu=u_\mu^\dagger=i(u^\dagger(\partial_\mu-ir_\mu)u-u(\partial_\mu-i\ell_\mu)u^\dagger)\\
&\chi=2B_0(s+ip)\ \chi^\dagger=2B_0(s-ip)\\
&\chi_\pm=\pm\chi_\pm^\dagger=u^\dagger\chi u^\dagger\pm u\chi^\dagger u\\
&\chi_-=i\chi_+|_{p\leftrightarrow s,u\leftrightarrow u^\dagger},
\end{aligned}\tag{A1}$$

where v_μ, a_μ are respectively vector and axial-vector sources, and s, p are respectively scalar and pseudoscalar sources. The local chiral transformations of the building block are the following:

$$\begin{aligned}
(L,R):u&=Ruh^\dagger(L,R,u)\\
&=h(L,R,u)L^\dagger\quad\text{where } h^\dagger h=1\\
(L,R):\ \ell_\mu&=L(\ell_\mu+i\partial_\mu)L^\dagger,\\
(L,R):\ r_\mu&=R(r_\mu+i\partial_\mu)R^\dagger\\
(L,R):\ u_\mu&=h(L,R,u)u_\mu h^\dagger(L,R,u)\\
(L,R):\ \chi_\pm&=h(L,R,u)\chi_\pm h^\dagger(L,R,u).
\end{aligned}\tag{A2}$$

For a matter field, in the present case a baryon, in a given irrep of isospin $SU(2)$, the chiral transformation law is the following:

$$(L(x),R(x)):\mathbf{B}(x)=h(L(x),R(x),u(x))\mathbf{B}(x),\tag{A3}$$

where the unitary h can be expressed as

$$h(L,R,u)=e^{i\alpha^a(L,R,u)I^a},\tag{A4}$$

with I^a in the given isospin irrep. For an isospin one operator X, its components X^a are given by $X^a=\frac{1}{2}\langle X\tau^a\rangle$, where $\langle\cdots\rangle$ represents the trace.

1. Expansion of building blocks

For the purpose of the present work the relevant terms in the building blocks are those with up to four-pion fields, namely:

$$\begin{aligned}
u_\mu&=2a_\mu-\frac{1}{F_\pi}\partial_\mu\Pi+\frac{i}{F_\pi}[v_\mu,\Pi]+\frac{1}{4F_\pi^2}[\Pi,[a_\mu,\Pi]]\\
&\quad+\frac{1}{24F_\pi^3}([\Pi,[\Pi,\partial_\mu\Pi]]-i[\Pi,[\Pi,[v_\mu,\Pi]]])+\cdots\\
u_\mu^a&=\frac{1}{2}\langle u_\mu\tau^a\rangle u_\mu\ \text{in the fundamental irrep}\\
\Gamma_\mu&=v_\mu+\frac{i}{2F_\pi}[a_\mu,\Pi]+\frac{i}{8F_\pi^2}[\Pi,[\partial_\mu-iv_\mu,\Pi]]\\
&\quad+\frac{i}{48F_\pi^3}[\Pi,[\Pi,[\Pi,a_\mu]]]\\
&\quad-\frac{i}{384F_\pi^4}[\Pi,[\Pi,[\Pi,[\partial_\mu-iv_\mu,\Pi]]]]+\cdots\\
\chi_+&=4B_0s+\frac{2B_0}{F_\pi}\{p,\Pi\}-\frac{B_0}{2F_\pi^2}\{\Pi,\{s,\Pi\}\}\\
&\quad-\frac{B_0}{12F_\pi^3}\{\Pi,\{\Pi,\{\Pi,p\}\}\}\\
&\quad+\frac{B_0}{96F_\pi^4}\{\Pi,\{\Pi,\{\Pi,\{\Pi,s\}\}\}\}+\cdots
\end{aligned}$$

$$\chi_- = i\Big(4B_0 p - \frac{2B_0}{F_\pi}\{s,\Pi\} - \frac{B_0}{2F_\pi^2}\{\Pi,\{p,\Pi\}\} + \frac{B_0}{12F_\pi^3}\{\Pi,\{\Pi,\{\Pi,s\}\}\} + \frac{B_0}{96F_\pi^4}\{\Pi,\{\Pi,\{\Pi,\{\Pi,p\}\}\}\} + \cdots\Big), \tag{A5}$$

where for the present work the following replacements are made: $p = 0$, $s = \mathcal{M}_q$, where $\mathcal{M}_q$ is the quark mass matrix, and $v^\mu = a^\mu = 0$. The following are useful explicit expansions in the pion fields of the building blocks:

$$\begin{aligned}
u_\mu^a &= -\frac{1}{F_\pi}\partial_\mu\pi^a + \frac{1}{6F_\pi^3}\pi^b(\pi^b \overleftrightarrow{\partial}_\mu \pi^a) + \cdots \\
u_\mu^a u_\nu^b &= \cdots + \frac{1}{F_\pi^2}\partial_\mu\pi^a\partial_\nu\pi^b + \cdots \\
\langle\chi_+\rangle &= \cdots + 4M_\pi^2 - \frac{2}{F_\pi^2}M_\pi^2\pi^a\pi^a + \frac{1}{6F_\pi^4}M_\pi^2\pi^a\pi^a\pi^b\pi^b + \cdots \\
\chi_+^a &= \frac{B_0(m_d - m_u)}{F_\pi^2}(\pi^a\pi^3 - 2F_\pi^2\delta^{a3}) + \cdots \\
\langle\chi_-\rangle &= \frac{4iB_0(m_d - m_u)\pi^3}{F_\pi} + \cdots \\
\chi_-^a &= -\frac{2iM_\pi^2\pi^a}{F_\pi} \\
D_\mu &= \partial_\mu + \frac{i}{2F_\pi^2}\epsilon^{abc}\pi^a\partial_\mu\pi^b I^c + \cdots \\
D_\mu D^\mu &= \partial_\mu\partial^\mu + \frac{i}{2F_\pi^2}\epsilon^{abc}I^c(\partial_\mu(\pi^a\partial^\mu\pi^b) + 2(\pi^a\partial_\mu\pi^b)\partial^\mu + \cdots).
\end{aligned} \tag{A6}$$

Additional bilinears in pion fields needed for the CTs are

$$\begin{aligned}
\langle\chi_+\rangle^2 &= 16M_\pi^4 - \frac{16}{F_\pi^2}M_\pi^4\pi^a\pi^a + \cdots \\
\langle\chi_+^2\rangle &= 8M_\pi^4 - \frac{2M_\pi^4}{F_\pi^2}\left(\frac{(m_d - m_u)^2}{\hat{m}^2}\pi^3\pi^3 + 4\pi^a\pi^a\right) + \cdots \\
\langle\chi_-\rangle^2 &= -\frac{16}{F_\pi^2}B_0^2(m_d - m_u)^2\pi^3\pi^3 + \cdots \\
\langle\chi_-^2\rangle &= -\frac{2M_\pi^4}{F_\pi^2}\left(\frac{(m_d - m_u)^2}{\hat{m}^2}\pi^3\pi^3 + 4\pi^a\pi^a\right) + \cdots,
\end{aligned} \tag{A7}$$

where $\hat{m} = \frac{1}{2}(m_u + m_d)$. Note that in this work, isospin symmetry is assumed.

2. Discrete symmetry transformations of building blocks

The Lagrangians respect the discrete P, C, and T symmetries, and the following Table II provides the necessary transformation rules for the building blocks.

TABLE II. P, C, and T transformation rules.

	P	C	T
x^μ	x_μ	x^μ	$-x_\mu$
∂^μ	∂_μ	∂^μ	$-\partial_\mu$
$\pi^a(x)$	$-\pi^a(P:x)$	$-(-1)^a\pi^a(x)$	$(-1)^a\pi^a(T:x)$
$u(x)$	$u^\dagger(P:x)$	$u^T(x)$	$u^*(T:x)$
$U(x)$	$U^\dagger(P:x)$	$U^T(x)$	$U^*(T:x)$
$\chi(x)$	$\chi^\dagger(P:x)$	$\chi^T(x)$	$\chi^*(T:x)$
$s(x)$	$s^\dagger(P:x)$	$s^T(x)$	$s^*(T:x)$
$p(x)$	$p^\dagger(P:x)$	$p^T(x)$	$p^*(T:x)$
$u^\mu(x)$	$-u_\mu^\dagger(P:x)$	$u^{\mu T}(x)$	$-u_\mu{}^*(T:x)$
$r^\mu(x)$	$\ell_\mu^\dagger(P:x)$	$-\ell^{\mu T}(x)$	$r_\mu^*(T:x)$
$\ell^\mu(x)$	$r_\mu^\dagger(P:x)$	$-r^{\mu T}(x)$	$\ell_\mu^*(T:x)$
$v^\mu(x)$	$v_\mu^\dagger(P:x)$	$-v^{\mu T}(x)$	$v_\mu^*(T:x)$
$a^\mu(x)$	$-a_\mu^\dagger(P:x)$	$a^{\mu T}(x)$	$a_\mu^*(T:x)$
$\mathbf{B}(x)$	$\mathbf{B}(P:x)$	$\cdots$	$e^{i\pi I^2}e^{i\pi S^2}\mathbf{B}(T:x)$
S^i	S^i	$\cdots$	S^{i*}
I^a	I^a	$\cdots$	I^{a*}
G^{ia}	G^{ia}	$\cdots$	G^{ia*}

Note that C does not apply to the baryon Lagrangians, as the heavy baryon expansion can only describe either baryons or antibaryons as separate sectors.

Under complex conjugation, the spin-flavor generators in an arbitrary representation satisfy the relations Eq. (B1):

$$\begin{aligned}
e^{-i\pi S^2}S^{i*}e^{i\pi S^2} &= -S^i \\
e^{-i\pi I^2}I^{a*}e^{i\pi I^2} &= -I^a \\
e^{-i\pi S^2}e^{-i\pi I^2}G^{ia*}e^{i\pi I^2}e^{i\pi S^2} &= G^{ia},
\end{aligned} \tag{A8}$$

where a, $i = 1, 2, 3$ and S^2 and I^2 are the respective generators with i, $a = 2$.

APPENDIX B: $SU(4)$ ALGEBRA

This appendix summarizes properties of the $SU(4)$ spin-flavor symmetry group used in the present analysis. The algebra of $SU(4)$ contains 15 generators: the spin generators S^i, the isospin generators I^a, and the spin-flavor generators G^{ia}, where i and a run from 1 to 3. The generator's commutation relations are the following:

$$\begin{aligned}
&[S^i, S^j] = i\epsilon^{ijk}S^k, \qquad [I^a, I^b] = i\epsilon^{abc}I^c, \\
&[I^a, S^i] = 0, \\
&[S^i, G^{ja}] = i\epsilon^{ijk}G^{ka}, \qquad [I^a, G^{ib}] = i\epsilon^{abc}G^{ic}, \\
&[G^{ia}, G^{jb}] = \frac{i}{4}\delta^{ij}\epsilon^{abc}I^c + \frac{i}{4}\delta^{ab}\epsilon^{ijk}S^k.
\end{aligned} \tag{B1}$$

The ground state baryons fill the $SU(4)$ totally symmetric irrep corresponding to the Young tableaux with N_c boxes of dimension $\frac{1}{6}(N_c+1)(N_c+2)(N_c+3)$. These states have

spin and isospin $S = I = \frac{1}{2}, \ldots, \frac{N_c}{2}$ and are denoted by $|SS_3I_3\rangle$. The matrix elements of the $SU(4)$ generators in these states are as follows:

$$\begin{aligned}
\langle S'S'_3I'_3|S^i|SS_3I_3\rangle &= \sqrt{S(S+1)}\delta_{S'S}\delta_{I'_3I_3}\langle SS_3, 1i|S'S'_3\rangle,\\
\langle S'S'_3I'_3|I^a|SS_3I_3\rangle &= \sqrt{S(S+1)}\delta_{S'S}\delta_{I'_3I_3}\langle SI_3, 1a|S'I'_3\rangle,\\
\langle S'S'_3I'_3|G^{ia}|SS_3I_3\rangle &= \frac{1}{4}\sqrt{\frac{2S+1}{2S'+1}}\\
&\quad\times\sqrt{(N_c+2)^2-(S-S')^2(S+S'+1)^2}\\
&\quad\times\langle SS_3, 1i|S'S'_3\rangle\langle SI_3, 1a|S'I'_3\rangle. \qquad \text{(B2)}
\end{aligned}$$

For states with $S = \mathcal{O}(N_c^0)$, S^i and I^a have matrix elements $\mathcal{O}(N_c^0)$ and connect only states with $S' = S$, while the generators G^{ia} have matrix elements $\mathcal{O}(N_c)$ and can connect states with $S' = S$ or $S \pm 1$.

TABLE III. $SU(4)$ operator identities in the totally symmetric irrep $(N_c, 0, 0)$ of $SU(4)$. The first column gives the composite operator's quantum numbers (J, I) under $SU(2) \times SU(2)$.

J	I	Relation
0	0	$\{S^i, S^i\} - \{I^a, I^a\} = 0$
0	0	$\{S^i, S^i\} + \{I^a, I^a\} + 4\{G^{ia}, G^{ia}\} = \frac{3}{2}N_c(4+N_c)$
0	1	$2\{S^i, G^{ia}\} = (2+N_c)I^a$
1	0	$2\{I^a, G^{ia}\} = (2+N_c)S^i$
1	1	$\frac{1}{2}\{S^k, I^c\} - \epsilon^{ijk}\epsilon^{abc}\{G^{ia}, G^{jb}\} = (2+N_c)G^{kc}$
1	1	$\epsilon^{ijk}\{S^i, G^{jc}\} = \epsilon^{abc}\{I^a, G^{kb}\}$
0	2	$4\{G^{ia}, G^{ib}\}\|_{I=2} = \{I^a, I^b\}\|_{I=2}$
2	0	$4\{G^{ia}, G^{ja}\}\|_{J=2} = \{S^i, S^j\}\|_{J=2}$

APPENDIX C: COMPOSITE SPIN-FLAVOR OPERATORS

An n-body spin-flavor composite operator is defined as the product of n generators of $SU(4)$. In an effective theory such operators will appear with a natural suppression factor $1/N_c^{n-1}$ [45,46]. For matrix elements in the totally symmetric irrep of $SU(4)$, the 2-body reduction relations in Table III are useful in the decomposition of higher body operators into bases operators. Composite operators can be projected onto definite spin and isospin irreducible tensors, in particular in building a suitable basis. Table IV gives the basis of composite operators needed in this work. The notations $X|_{J,I}$ indicate projection of the tensor X onto given quantum numbers (J, I). The spin-flavor tensors of the UV divergencies of the one-loop diagrams can always be expressed in terms of those bases operators. This is not the case for the nonanalytic terms, which will require explicit evaluations for each of the projections on intermediate baryon states in the loop. For the case of $\pi N \to \pi N$, Appendix F 6 shows those evaluations.

APPENDIX D: LAGRANGIANS

This appendix gives the chiral Lagrangians needed in this work, namely the LO Lagrangian for pions, and the LO, NLO, and NNLO for baryons, which only include those terms necessary for a complete renormalization of the $\pi B \to \pi B'$ scattering amplitudes. The baryon Lagrangians are organized according the ξ power counting.

1. LO Lagrangians

The pion LO Lagrangian $\mathcal{O}(p^2) = \mathcal{O}(\xi^2)$ has the standard form:

TABLE IV. Spin-flavor tensor operator basis. To complete the basis to the terms in the table additional terms involving anticommutators of those terms with $\frac{1}{N_c^2} \times \hat{S}^2$ must be added. Most of those terms will be of higher order than the ones needed for renormalizing the scattering amplitudes.

J	I	Operator	J	I	Operator
0	0	1	2	1	$\frac{1}{N_c^2}S^iS^j\|_{J=2}I^a$
1	0	S^i	2	1	$\frac{1}{N_c^2}\{S^iS^j\|_{J=2}, G^{ka}\}\|_{J=2,I=1}$
0	1	I^a	1	2	$\frac{1}{N_c}\{I^a, G^{ib}\}\|_{I=2}$
1	1	G^{ia}	1	2	$\frac{1}{N_c^2}\{S^iI^a, G^{jb}\}\|_{J=1,I=2}$
1	1	$\frac{1}{N_c}S^iI^a$	1	2	$\frac{1}{N_c^2}S^iI^aI^b\|_{I=2}$
1	1	$\frac{1}{N_c}\{S^i, G^{ja}\}\|_{J=1}$	1	2	$\frac{1}{N_c^2}\{I^aI^b\|_{I=2}, G^{ic}\}\|_{J=1,I=2}$
2	0	$\frac{1}{N_c}S^iS^j\|_{J=2}$	2	2	$\frac{1}{N_c}\{G^{ia}, G^{jb}\}\|_{J=I=2}$
0	2	$\frac{1}{N_c}I^aI^b\|_{I=2}$	2	2	$\frac{1}{N_c^2}\{S^iI^a, G^{jb}\}\|_{J=I=2}$
2	1	$\frac{1}{N_c}\{S^i, G^{ja}\}\|_{J=2}$	2	2	$\frac{1}{N_c^2}\{S^i, G^{ja}G^{kb}\|_{J=I=2}\}\|_{J=I=2}$
2	1	$\frac{1}{N_c^2}\{S^iI^a, G^{jb}\}\|_{J=2,I=1}$	2	2	$\frac{1}{N_c^3}S^iS^j\|_{J=2}I^aI^b\|_{I=2}$

TABLE V. Vertices from the LO Lagrangians.

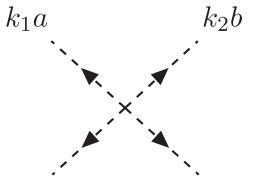	$= \frac{i}{3F_\pi^2}(M_\pi^2(\delta^{ab}\delta^{cd}+\delta^{ac}\delta^{bd}+\delta^{ad}\delta^{bc})$ $+\delta^{ab}\delta^{cd}(-(k_1+k_2)\cdot(k_3+k_4)+2(k_1\cdot k_2+k_3\cdot k_4))$ $+\delta^{ac}\delta^{bd}(-(k_1+k_3)\cdot(k_2+k_4)+2(k_1\cdot k_3+k_2\cdot k_4))$ $+\delta^{ad}\delta^{bc}(-(k_2+k_3)\cdot(k_1+k_4)+2(k_1\cdot k_4+k_2\cdot k_3)))$
	$= \frac{\mathring{g}_A}{F_\pi} k^i G^{ia}$
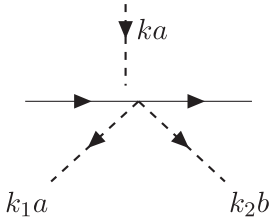	$= \frac{1}{F_\pi^2}(\frac{1}{2}(k_2^0-k_1^0)\epsilon^{abc}I^c - i2c_1N_c\frac{M_\pi^2}{\Lambda}\delta^{ab})$
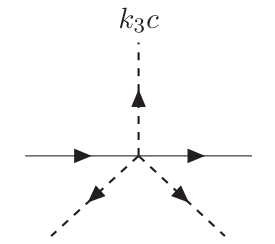	$= -\frac{\mathring{g}_A}{F_\pi^2}G^{id}(\delta^{ab}\delta^{cd}(2k_3^i-k_1^i-k_2^i)+\delta^{ac}\delta^{bd}(2k_2^i-k_1^i-k_3^i)$ $+\delta^{ad}\delta^{bc}(2k_1^i-k_2^i-k_3^i))$
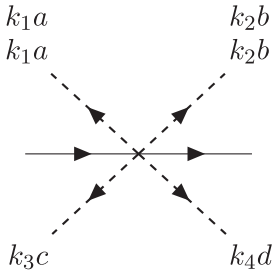	$= \frac{1}{F_\pi^4}(\frac{1}{12}I^e(\delta^{ab}\epsilon^{cde}(k_3^0-k_4^0)+\delta^{ac}\epsilon^{bde}(k_2^0-k_4^0)+\delta^{ad}\epsilon^{bce}(k_2^0-k_3^0)$ $+\delta^{bc}\epsilon^{ade}(k_1^0-k_4^0)+\delta^{bd}\epsilon^{ace}(k_1^0-k_3^0)+\delta^{cd}\epsilon^{abe}(k_1^0-k_2^0))$ $+i\frac{2}{3}c_1N_c\frac{M_\pi^2}{\Lambda}(\delta^{ab}\delta^{cd}+\delta^{ac}\delta^{bd}+\delta^{ad}\delta^{bc}))$

$$\mathcal{L}_\pi^{(2)} = \frac{1}{4}F_\pi^2\langle D_\mu U^\dagger D^\mu U + \chi U^\dagger + \chi^\dagger U\rangle. \tag{D1}$$

The LO baryon Lagrangian is $\mathcal{O}(\xi)$ and given by

$$\mathcal{L}_B^{(1)} = \mathbf{B}^\dagger\left(iD_0 + \mathring{g}_A u^{ia}G^{ia} - \frac{C_{HF}}{N_c}\hat{S}^2 + \frac{c_1N_c}{2\Lambda}\langle\chi_+\rangle\right)\mathbf{B}. \tag{D2}$$

The vertices from the LO Lagrangian needed in the NLO and NNLO calculations are depicted in Table V.

2. Higher order Lagrangians

In the construction of the higher order Lagrangians one uses the LO equations of motion, namely,

$$iD_0\mathbf{B} = \left(\frac{C_{\rm HF}}{N_c}\hat{S}^2 - c_1\frac{N_c}{2\Lambda}\langle\chi_+\rangle - \mathring{g}_A u^{ia}G^{ia}\right)\mathbf{B}$$
$$D_\mu u^\mu = \frac{i}{2}\chi_-, \tag{D3}$$

and the identities,

$$D_\mu u_\nu - D_\nu u_\mu = -f_{-\mu\nu}$$
$$[D_\mu, D_\nu] = -i\Gamma_{\mu\nu}$$
$$\Gamma_{\mu\nu} = \frac{1}{2}f_{+\mu\nu} + \frac{i}{4}[u_\mu, u_\nu]. \tag{D4}$$

The following are the higher order Lagrangians needed for renormalization in the present calculation of the $\pi B \to \pi B'$ amplitudes. The CT Lagrangians needed to renormalize UV divergencies are organized by the order in $\mathring{g}_A$ of the UV divergencies, and are the following:

$$\mathcal{L}_{\rm CT}(\mathring{g}_A^4) = \mathbf{B}^\dagger\Bigg(\frac{f_{10}}{\Lambda^2}\epsilon^{ijk}S^k u^{ia}\overset{\leftrightarrow}{D}_0 u^{ja} + \frac{f_{01}}{\Lambda^2}\epsilon^{abc}I^c u^{ia}\overset{\leftrightarrow}{D}_0 u^{ib} + \frac{f_{11}^{(1)}}{\Lambda}\epsilon^{ijk}\epsilon^{abc}u^{ia}u^{jb}G^{kc} + \frac{f_{11}^{(2)}}{\Lambda}\epsilon^{ijk}\epsilon^{abc}u^{ia}u^{jb}\frac{1}{N_c}S^k I^c$$
$$+ \frac{f_{20}}{\Lambda}u^{ia}u^{ja}\frac{1}{N_c}S^iS^j\Big|_{J=2} + \frac{f_{02}}{\Lambda}u^{ia}u^{ib}\frac{1}{N_c}I^aI^b\Big|_{I=2} + \frac{f_{22}}{\Lambda}u^{ia}u^{jb}\frac{1}{N_c}G^{ia}G^{jb}\Big|_{J=I=2}\Bigg)\mathbf{B} \tag{D5}$$

$$\mathcal{L}_{\rm CT}(\mathring{g}_A^2) = \mathbf{B}^\dagger\Bigg(g_{00}^{(1)}\frac{\langle\chi_+\rangle}{\Lambda} + g_{00}^{(2)}\frac{\langle\chi_+\rangle}{\Lambda}\frac{\hat{S}^2}{N_c} + \frac{g_{00}^{(3)}}{\Lambda}u_\mu^a u^{a\mu} + \frac{g_{00}^{(4)}}{\Lambda}u_\mu^a u^{a\mu}\frac{\hat{S}^2}{N_c} + i\frac{g_{01}^{(1)}}{\Lambda^2}\epsilon^{abc}\chi_-^a u_0^b I^c + \frac{g_{01}^{(2)}}{\Lambda^2}\epsilon^{abc}u_\mu^a\overset{\leftrightarrow}{D}_0 u^{b\mu}I^c$$
$$+ \frac{g_{02}^{(1)}}{\Lambda}u_\mu^a u^{b\mu}I^aI^b\Big|_{I=2} + \frac{g_{11}^{(1)}}{\Lambda}\epsilon^{ijk}\epsilon^{abc}u^{ia}u^{jb}G^{kc} + \frac{g_{11}^{(2)}}{\Lambda}\epsilon^{ijk}\epsilon^{abc}u^{ia}u^{jb}\frac{1}{N_c}S^kI^c\Bigg)\mathbf{B} \tag{D6}$$

$$\mathcal{L}_{\rm CT}(\mathring{g}_A^0) = \mathbf{B}^\dagger\Bigg(h_{00}^{(1)}\frac{N_c}{\Lambda^3}\langle\chi_+^2\rangle + h_{00}^{(2)}\frac{N_c}{\Lambda^3}\langle\chi_-^2\rangle + h_{00}^{(3)}\frac{N_c}{\Lambda^3}\langle\chi_+\rangle u_\mu^a u^{\mu a} + ih_{01}^{(1)}\frac{\epsilon^{abc}}{\Lambda^2}\chi_-^a u_0^b I^c + h_{01}^{(2)}\frac{\epsilon^{abc}}{\Lambda^2}u_\mu^a\overset{\leftrightarrow}{D}_0 u^{\mu b}I^c$$
$$+ h_{01}^{(3)}\frac{\epsilon^{abc}}{\Lambda^2}u_0^a\overset{\leftrightarrow}{D}_0 u_0^b I^c\Bigg)\mathbf{B}. \tag{D7}$$

The LEC notation explicitly gives the (J, I) of the spin-flavor tensor, namely, LEC_{JI}. Note that a few terms have the same structure across the depicted Lagrangians, thus the corresponding LECs add up. They have been presented separately because in the renormalization the corresponding β functions are organized in powers of $\mathring{g}_A$.

In addition, and to the order of the present calculations, there are Lagrangian terms that serve as finite CTs. Here again only those contributing to the $\pi B \to \pi B'$ amplitudes are shown:

$$\mathcal{L}_{\rm CT}(\text{finite}) = i\frac{\ell_{00}^{(1)}}{\Lambda^2}u_0^a u^{ia}\mathbf{B}^\dagger\overset{\leftrightarrow}{D}^i\mathbf{B} + i\frac{\ell_{00}^{(2)}}{\Lambda^2}\langle\chi_+\rangle\mathbf{B}^\dagger\overset{\leftrightarrow}{D}_0\mathbf{B} + \ell_{01}^{(1)}\frac{1}{2m_0}\mathbf{B}^\dagger\vec{D}^2\mathbf{B} + \frac{\ell_{01}^{(2)}}{\Lambda^2}\epsilon^{abc}u^{ia}D^i u_0^b\mathbf{B}^\dagger I^c\mathbf{B}$$
$$+ \frac{\ell_{01}^{(3)}}{\Lambda^2}\epsilon^{abc}D^i u^{ia}u_0^b\mathbf{B}^\dagger I^c\mathbf{B} + \frac{\ell_{10}^{(1)}}{\Lambda^2}\epsilon^{ijk}u^{ia}D^j u_0^a\mathbf{B}^\dagger S^k\mathbf{B} + \frac{\ell_{10}^{(2)}}{\Lambda^2}\epsilon^{ijk}D^j u^{ia}u_0^a\mathbf{B}^\dagger S^k\mathbf{B}$$
$$+ i\frac{\ell_{11}^{(1)}}{2\Lambda^2}\epsilon^{ijk}\epsilon^{abc}u_0^a u^{ib}\mathbf{B}^\dagger\{\overset{\leftrightarrow}{D}^j, G^{kc}\}\mathbf{B} + i\frac{\ell_{11}^{(2)}}{2\Lambda^2}\epsilon^{ijk}\epsilon^{abc}u^{ia}u^{jb}\mathbf{B}^\dagger\{\overset{\leftrightarrow}{D}_0, G^{kc}\}\mathbf{B}$$
$$+ \text{terms with either } J \text{ or } I \text{ bigger than1}, \tag{D8}$$

where the terms not contributing to the $\pi N \to \pi N$ amplitude are not explicitly shown, i.e. terms where J or I are larger than 1.

For the contributions to the scattering amplitudes, the renormalization of the baryon masses and the πB couplings are needed. The corresponding CT Lagrangians are the following:

$$\mathcal{L}_m^{\rm CT} = \mathbf{B}^\dagger\Bigg(\frac{C_{HF1}}{N_c^2}\hat{S}^2 + \frac{C_{HF2}}{N_c^3}\hat{S}^4 + \frac{c_2}{N_c}\langle\chi_+\rangle\hat{S}^2\Bigg)\mathbf{B}. \tag{D9}$$

$$\mathcal{L}_A^{\rm CT} = \mathbf{B}^\dagger\Bigg(u_{ia}\Bigg(\frac{C_0^A}{N_c}G^{ia} + \frac{C_1^A}{4\Lambda^2}\{\chi_+, G^{ia}\} + \frac{C_2^A}{N_c^2}\{\hat{S}^2, G^{ia}\} + \frac{C_3^A}{N_c}[\hat{S}^2, G^{ia}] + \frac{C_4^A}{N_c}S^iI^a\Bigg) + i\frac{C_5^A}{2\Lambda^2}D^i\chi_-^a G^{ia}\Bigg)\mathbf{B}$$
$$+ i\frac{\mathring{g}_A}{m_0}u^{0a}\mathbf{B}^\dagger\{G^{ia}, \overset{\leftrightarrow}{D}^i\}\mathbf{B}. \tag{D10}$$

This Lagrangian provides the renormalization CTs for both the axial current and the πB interaction. The loop correction preserves the Goldberger-Treiman relation, whose discrepancy is only due to the term proportional to C_5^A. The term proportional to $\mathring{g}_A/m_0$, demanded by the nonrelativistic expansion, gives the leading contribution to the time component of the axial current and the corresponding pion-baryon coupling, giving contributions $\mathcal{O}(\xi^2)$ with respect to the spatial components of the axial current. Although these contributions to the pion-baryon coupling are NNLO, they are found to be virtually insignificant and are thus disregarded in the fits to the data.

APPENDIX E: LOOP INTEGRALS

This appendix gives details on the loop integrals, where throughout dimensional regularization is used, with $d = 4 - 2\epsilon$, and the notation $\lambda_\epsilon \equiv \frac{1}{\epsilon} - \gamma_E + \log 4\pi$.

All one-loop integrals, after convenient integration variable shifts, can be brought to the following general well known forms, leaving integrations over Feynman parameters to be performed:

$$\int \widetilde{d^d k} \frac{\{1; k^\mu k^\nu; \cdots\}}{(k^2 - \Lambda^2 + i\epsilon)^n}, \tag{E1}$$

where $\widetilde{d^d k} = \frac{d^d k}{(2\pi)^d}$, and Λ contains in particular dependencies on Feynman parameters.

Diagrams not involving heavy baryon propagators lead straightforwardly to the integral forms shown above. When heavy baryon propagators are involved, the general form of the loop integrals are obtained by first using the Feynman parameter representation:

$$\begin{aligned}\frac{1}{A_1 \cdots A_m a_1 \cdots a_n} = 2^m \Gamma(m+n) \int_0^1 d\alpha_1 \int_0^1 d\alpha_2 \cdots \int_0^1 d\alpha_n \\ \times \int_0^\infty d\lambda_1 \cdots \int_0^\infty d\lambda_m \frac{\delta(1 - \alpha_1 - \cdots - \alpha_n)}{(2\lambda_1 A_1 + \cdots + \alpha_1 a_1 + \cdots)^{(n+m)}}.\end{aligned} \tag{E2}$$

The cases needed in this work are those with one, two, and three heavy baryon propagators. All cases can be brought to the case with a single heavy baryon propagator using the partial fraction decomposition. Thus the integrals of interest will be of the general form

$$\begin{aligned}&\int \widetilde{d^d k} \frac{\mathrm{Num}(k, \{q_i\})}{(Q^0 - k^0 + i\epsilon)(k^2 - M_\pi^2 + i\epsilon)((k-q_1)^2 - M_\pi^2 + i\epsilon) \cdots ((k-q_n)^2 - M_\pi^2 + i\epsilon)} \\ &= 2\Gamma(n) \int_0^\infty d\lambda \int_0^1 d\alpha_1 \cdots d\alpha_n \int \widetilde{d^d k} \frac{\delta(1 - \alpha_1 - \cdots - \alpha_n)\mathrm{Num}(k, \{q_i\})}{(2\lambda(Q^0 - k^0 + i\epsilon) + \sum_i^n \alpha_i((k-q_i)^2 - M_\pi^2 + i\epsilon))^{n+1}},\end{aligned} \tag{E3}$$

where Num is a polynomial of the arguments. Upon integrating over k, the integration over the Feynman parameter λ has the general form

$$J(r, \nu, C_0, C_1, \lambda_0) \equiv \int_0^\infty d\lambda \frac{\lambda^r}{(C_0 + C_1(\lambda - \lambda_0)^2)^\nu}, \tag{E4}$$

where $r = 0, 1, \ldots$, and $\nu = \text{integer} - \frac{d}{2}$.

The integrals $J(r, \nu, C_0, C_1, \lambda_0)$ satisfy the following recurrence relations:

$$\begin{aligned}J(0, \nu, C_0, C_1, \lambda_0) &= \frac{1}{2\nu - 1}\left(2\nu C_0 J(0, \nu+1, C_0, C_1, \lambda_0) - \frac{\lambda_0}{(C_0 + C_1\lambda_0^2)^\nu}\right) \\ J(1, \nu, C_0, C_1, \lambda_0) &= \lambda_0 J(0, \nu, C_0, C_1, \lambda_0) + \frac{(C_0 + C_1\lambda_0^2)^{1-\nu}}{2C_1(\nu - 1)} \\ J(2, \nu, C_0, C_1, \lambda_0) &= (\lambda_0^2 - C_0) J(0, \nu, C_0, C_1, \lambda_0) + J(0, \nu - 1, C_0, C_1, \lambda_0) + \lambda_0 \frac{(C_0 + C_1\lambda_0^2)^{1-\nu}}{2C_1(\nu - 1)}\end{aligned} \tag{E5}$$

The seed integral is taken to be the one for $\nu = 1 + \epsilon$:

$$J(0, 1+\epsilon, C_0, C_1, \lambda_0) = \frac{1}{\sqrt{C_0 C_1}}\left(\frac{\pi}{2} + \arctan\frac{\lambda_0}{\sqrt{C_0/C_1}}\right) - \epsilon \int_0^\infty \frac{\log(C_0 + C_1(\lambda - \lambda_0)^2)}{C_0 + C_1(\lambda - \lambda_0)^2} d\lambda. \tag{E6}$$

The integrals $J(0, n + \epsilon, C_0, C_1, \lambda_0)$ with $n = 0, -1, -2, \ldots$ are polynomials in C_0, C_1, and λ_0, while for $n > 0$ they do contain nonanalytic terms. In general, the integrals always appear in the one-loop results in the combination $\Gamma(\nu) J(n, \nu, C_0, C_1, \lambda_0)$. In the actual calculations of this work, it turns out that $C_1 = 1$ throughout.

TABLE VI. Integrals over the Feynman parameter λ.

r	ν	$\Gamma(\nu+\epsilon)J(r,\nu+\epsilon,C_0,C_1,\lambda_0)$
0	0	$\frac{1}{2}(\lambda_0^2-\frac{C_0}{C_1})\lambda_\epsilon-\frac{\sqrt{C_0C_1}\lambda_0(2\arctan(\sqrt{\frac{C_1}{C_0}}\lambda_0)+\pi)}{C_1}+\frac{3C_1\lambda_0^2-C_0+(C_0-C_1\lambda_0^2)\log(C_1\lambda_0^2+C_0)}{2C_1}$
0	1	$\frac{\lambda_\epsilon}{2C_1}+\frac{\lambda_0(2\arctan(\sqrt{\frac{C_1}{C_0}}\lambda_0)+\pi)}{2\sqrt{C_0C_1}}-\frac{\log(C_1\lambda_0^2+C_0)}{2C_1}$
0	2	$\frac{\lambda_0(2\arctan(\sqrt{\frac{C_1}{C_0}}\lambda_0)+\pi)}{4C_0\sqrt{C_0C_1}}+\frac{1}{2C_0C_1}$
0	3	$\frac{3C_1\lambda_0^2+2C_0}{4C_0^2C_1(C_1\lambda_0^2+C_0)}+\frac{3\lambda_0(2\arctan(\sqrt{\frac{C_1}{C_0}}\lambda_0)+\pi)}{8C_0^2\sqrt{C_0C_1}}$
1	0	$\frac{1}{2}(\lambda_0^2-\frac{C_0}{C_1})\lambda_\epsilon-\frac{\sqrt{C_0C_1}\lambda_0(2\arctan(\sqrt{\frac{C_1}{C_0}}\lambda_0)+\pi)}{C_1}+\frac{3C_1\lambda_0^2-C_0+(C_0-C_1\lambda_0^2)\log(C_1\lambda_0^2+C_0)}{2C_1}$
1	1	$\frac{\lambda_\epsilon}{2C_1}+\frac{\lambda_0(2\arctan(\sqrt{\frac{C_1}{C_0}}\lambda_0)+\pi)}{2\sqrt{C_0C_1}}-\frac{\log(C_1\lambda_0^2+C_0)}{2C_1}$
1	2	$\frac{\lambda_0(2\arctan(\sqrt{\frac{C_1}{C_0}}\lambda_0)+\pi)}{4C_0\sqrt{C_0C_1}}+\frac{1}{2C_0C_1}$
1	3	$\frac{3C_1\lambda_0^2+2C_0}{4C_0^2C_1(C_1\lambda_0^2+C_0)}+\frac{3\lambda_0(2\arctan(\sqrt{\frac{C_1}{C_0}}\lambda_0)+\pi)}{8C_0^2\sqrt{C_0C_1}}$
2	0	$\frac{1}{2}(\lambda_0^2-\frac{C_0}{C_1})\lambda_\epsilon-\frac{\sqrt{C_0C_1}\lambda_0(2\arctan(\sqrt{\frac{C_1}{C_0}}\lambda_0)+\pi)}{C_1}+\frac{3C_1\lambda_0^2-C_0+(C_0-C_1\lambda_0^2)\log(C_1\lambda_0^2+C_0)}{2C_1}$
2	1	$\frac{\lambda_\epsilon}{2C_1}+\frac{\lambda_0(2\arctan(\sqrt{\frac{C_1}{C_0}}\lambda_0)+\pi)}{2\sqrt{C_0C_1}}-\frac{\log(C_1\lambda_0^2+C_0)}{2C_1}$
2	2	$\frac{\lambda_0(2\arctan(\sqrt{\frac{C_1}{C_0}}\lambda_0)+\pi)}{4C_0\sqrt{C_0C_1}}+\frac{1}{2C_0C_1}$
2	3	$\frac{3C_1\lambda_0^2+2C_0}{4C_0^2C_1(C_1\lambda_0^2+C_0)}+\frac{3\lambda_0(2\arctan(\sqrt{\frac{C_1}{C_0}}\lambda_0)+\pi)}{8C_0^2\sqrt{C_0C_1}}$

With these results, Table VI yields the necessary λ-Feynman parameter integrals for the present one-loop calculations. A particular integral, which is convenient to display explicitly is

$$\begin{aligned}\mathcal{I}(Q,M_\pi)&=\frac{1}{d-1}\int\widetilde{d^dk}\frac{\vec{k}^2}{(k^0-Q+i\epsilon)(k^2-M_\pi^2+i\epsilon)}\\&=\frac{i}{3(4\pi)^2}\left(Q\left((3M_\pi^2-2Q^2)\left(\lambda_\epsilon-\log\frac{M_\pi^2}{\mu^2}\right)+7M_\pi^2-\frac{16}{3}Q^2\right)\right.\\&\quad\left.+4\left(M_\pi^2-Q^2-i\epsilon\right)^{3/2}\left(\frac{\pi}{2}-\arctan\frac{Q}{\sqrt{M_\pi^2-Q^2-i\epsilon}}\right)\right).\end{aligned}\tag{E7}$$

This integral appears in the self-energy and in several of the one-loop contributions to the scattering amplitude.

APPENDIX F: NNLO SCATTERING AMPLITUDES

This appendix gives details of the calculations of the one-loop diagrams for the scattering amplitudes, organized by their power in $\mathring{g}_A$. The UV divergent pieces are analyzed in detail for the purpose of demonstrating the large N_c consistency of the results. Also included are the higher order Lagrangian contributions to the amplitudes, as well as the results for the β functions of the LECs. The simplifications for the case of $\pi N\to\pi N$ scattering are also included, along with results for the reductions of composite spin-flavor tensors needed in that case.

The case of $\pi N\to\pi N$ scattering shows significant simplifications, shown explicitly for the CT contributions. The reductions of composite spin-flavor tensors needed in that case are also included in Appendix F 6.

1. Diagrams $\propto \mathring{g}_A^4$

The diagrams proportional to $\mathring{g}_A^4$ are shown in Fig. 5. Diagrams D_1, D_2, and D_3 will contribute with pole terms, i.e., terms that contain singularities due to a single baryon pole. Diagram D_1 has double pole, single pole, and no-pole contributions, while diagrams D_2 and D_3 have single-pole and no-pole contributions.

First consider diagrams D_2: they have the general structure of a diagram shown in Fig. 10(a). The amplitude corresponding to that diagram reads

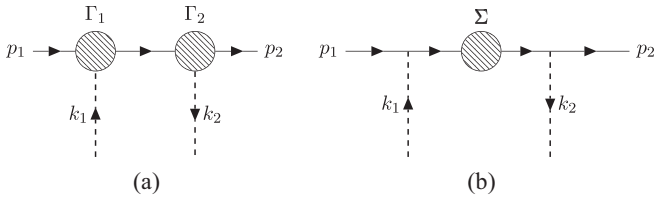

FIG. 10. Pole diagrams.

$$
\begin{aligned}
iT(a) &= -\frac{i}{p_1^0+k_1^0-\delta m_n}\Gamma_2(p_1^0+k_1^0,p_2^0,k_2)\mathcal{P}_n\Gamma_1(p_1^0,p_1^0+k_1^0,-k_1)\\
&= -i\Bigg(\frac{\Gamma_2(\delta m_n,p_2^0,k_2)\mathcal{P}_n\Gamma_1(p_1^0,\delta m_n,-k_1)}{p_1^0+k_1^0-\delta m_n}\\
&\quad+\frac{\Gamma_2(p_1^0+k_1^0,p_2^0,k_2)\mathcal{P}_n\Gamma_1(p_1^0,p_1^0+k_1^0,-k_1)-\Gamma_2(\delta m_n,p_2^0,k_2)\mathcal{P}_n\Gamma_1(p_1^0,\delta m_n,-k_1)}{p_1^0+k_1^0-\delta m_n}\Bigg),
\end{aligned}
\tag{F1}
$$

where in the last expression the first term contains a pole and the last one does not. When renormalizing, the first term will only require the renormalization of the vertices, while the last one will require renormalization of the scattering amplitudes, i.e., local terms with two pions.

The case of the diagram Fig. 10(b) with double pole is decomposed into terms with double pole, single pole and no pole, namely,

$$
\begin{aligned}
iT(b) &= \Gamma_2\mathcal{P}_n\Sigma(p_1^0+k_1^0)\mathcal{P}_n\Gamma_1\frac{1}{(p_1^0+k_1^0-\delta m_n)^2}\\
&= \frac{1}{(p_1^0+k_1^0-\delta m_n)^2}\Gamma_2\mathcal{P}_n(\Sigma(\delta m_n)+(p_1^0+k_1^0-\delta m_n)\Sigma'(\delta m_n)\\
&\quad+(\Sigma(p_1^0+k_1^0)-\Sigma(\delta m_n)-(p_1^0+k_1^0-\delta m_n)\Sigma'(\delta m_n)))\mathcal{P}_n\Gamma_1,
\end{aligned}
\tag{F2}
$$

where one identifies $\Sigma'(\delta m_n)=-\delta Z(\delta m_n)$. The first term has a double pole which is taken care of by the mass renormalization, the second term has a single pole, and the last one has no pole. For the single pole term the renormalization is through the vertex renormalization.

Applying those decompositions to the corresponding diagrams leads to the following results:

Diagram D_1:

$$
\begin{aligned}
iT^{ba}_{D_1} &= -i\left(\frac{\mathring{g}_A}{F_\pi}\right)^2 k_1^i k_2^j\sum_n G^{jb}\mathcal{P}_n G^{ia}\frac{\Sigma_n(p_1^0+k_1^0)}{(p_1^0+k_1^0-\delta m_n)^2}\\
&= -i\left(\frac{\mathring{g}_A}{F_\pi}\right)^2 k_1^i k_2^j\sum_n G^{jb}\mathcal{P}_n G^{ia}\left(\frac{\Sigma_n(\delta m_n)}{(p_1^0+k_1^0-\delta m_n)^2}-\frac{\delta Z_n(\delta m_n)}{p_1^0+k_1^0-\delta m_n}+\frac{\Sigma_n(p_1^0+k_1^0)-\Sigma_n(\delta m_n)}{(p_1^0+k_1^0-\delta m_n)^2}+\frac{\delta Z_n(\delta m_n)}{p_1^0+k_1^0-\delta m_n}\right).
\end{aligned}
\tag{F3}
$$

Diagrams D_2:

$$\begin{aligned} iT^{ba}_{D_2} &= \frac{\mathring{g}_A}{F_\pi} k_1^i k_2^j \sum_n \frac{1}{p_1^0 + k_1^0 - \delta m_n} (G^{jb}\mathcal{P}_n \Gamma^{ia}(p_1^0, p_1^0 + k_1^0, -k_1) + \Gamma^{jb}(p_1^0 + k_1^0, p_2^0, k_2)\mathcal{P}_n G^{ia}) \\ &= \frac{\mathring{g}_A}{F_\pi} k_1^i k_2^j \sum_n \frac{1}{p_1^0 + k_1^0 - \delta m_n} (G^{jb}\mathcal{P}_n \Gamma^{ia}(p_1^0, \delta m_n, -k_1) + \Gamma^{jb}(\delta m_n, p_2^0, k_2)\mathcal{P}_n G^{ia} \\ &\quad + (G^{jb}\mathcal{P}_n(\Gamma^{ia}(p_1^0, p_1^0 + k_1^0, -k_1) - \Gamma^{ia}(p_1^0, \delta m_n, -k_1)) \\ &\quad + (\Gamma^{jb}(p_1^0 + k_1^0, p_2^0, k_2) - \Gamma^{jb}(\delta m_n, p_2^0, k_2))\mathcal{P}_n G^{ia})). \end{aligned} \tag{F4}$$

Diagrams D_3:

$$\begin{aligned} iT^{ba}_{D_3} = -i\left(\frac{\mathring{g}_A}{F_\pi}\right)^2 k_1^i k_2^j \sum_n G^{jb}\mathcal{P}_n G^{ia} \frac{1}{p_1^0 + k_1^0 - \delta m_n} \left(\frac{\Sigma_{\text{in}}(\delta m_{\text{in}})}{p_1^0 - \delta m_{\text{in}}} + \frac{(\Sigma_{\text{out}}(\delta m_{\text{out}})}{p_2^0 - \delta m_{\text{out}}}\right. \\ \left. + \frac{\Sigma_{\text{in}}(p_1^0) - \Sigma_{\text{in}}(\delta m_{\text{in}}}{p_1^0 - \delta m_{\text{in}}} + \frac{\Sigma_{\text{out}}(p_2^0) - \Sigma_{\text{out}}(\delta m_{\text{out}})}{p_2^0 - \delta m_{\text{out}}}\right) \end{aligned} \tag{F5}$$

The term with external pole will be absorbed by renormalizing the baryon masses of the external baryons, and the terms with no external pole multiplied by $1/2$, which are a consequence of the external Baryon's wave function renormalization, are part of the scattering amplitude, which reduces to

$$iT^{ba}_{D_3} = \frac{i}{2}\left(\frac{\mathring{g}_A}{F_\pi}\right)^2 k_1^i k_2^j \sum_n \frac{1}{p_1^0 + k_1^0 - \delta m_n} \{G^{jb}\mathcal{P}_n G^{ia}, \delta\hat{Z}\} \tag{F6}$$

Diagram D_4:

$$\begin{aligned} T^{ba}_{D_4} = \left(\frac{\mathring{g}_A}{F_\pi}\right)^4 k_1^i k_2^j \sum_{n,n',n''} G^{lc}\mathcal{P}_{n''} G^{jb}\mathcal{P}_{n'} G^{ia}\mathcal{P}_n G^{lc} \left(\frac{\mathcal{I}(\delta m_n - p_1^0, M_\pi)}{(p_2^0 - p_1^0 - \delta m_{n''} + \delta m_n)(k_1^0 + \delta m_n - \delta m_{n'})}\right. \\ + \frac{\mathcal{I}(\delta m_{n''} - p_2^0, M_\pi)}{(p_2^0 - p_1^0 - \delta m_{n''} + \delta m_n)(p_2^0 - p_1^0 - k_1^0 - \delta m_{n''} + \delta m_{n'})} \\ \left. - \frac{\mathcal{I}(\delta m_{n'} - p_1^0 - k_1^0, M_\pi)}{(p_2^0 - p_1^0 - k_1^0 - \delta m_{n''} + \delta m_{n'})(k_1^0 + \delta m_n - \delta m_{n'})}\right). \end{aligned} \tag{F7}$$

a. UV divergencies of the no-pole terms

The UV divergent terms of the no-pole terms of the diagrams proportional to $\mathring{g}_A^4$ are as follows:
Diagram D_1 UV:

$$\begin{aligned} iT^{ba^{\text{UV}}}_{(D_1)}(\text{no-pole}) &= i\frac{\lambda_\epsilon}{(4\pi)^2}\left(\frac{\mathring{g}_A}{F_\pi}\right)^4 \frac{2}{3} k_1^i k_2^j \sum_{n,n'} \left(\frac{1}{2}(k_1^0 + k_2^0) + \frac{1}{2}(\delta m_{\text{in}} + \delta m_{\text{out}}) + 2\delta m_n - 3\delta m_{n'}\right) G^{jb}\mathcal{P}_n G^{lc}\mathcal{P}_{n'} G^{lc}\mathcal{P}_n G^{ia} \\ &= i\frac{\lambda_\epsilon}{(4\pi)^2}\left(\frac{\mathring{g}_A}{F_\pi}\right)^4 \frac{1}{3} k_1^i k_2^j ((k_1^0 + k_2^0) G^{jb}\hat{G}^2 G^{ia} + [\delta\hat{m}, G^{jb}]\hat{G}^2 G^{ia} \\ &\quad - G^{jb}\hat{G}^2[\delta\hat{m}, G^{ia}] + 3G^{ib}[[\delta\hat{m}, G^{lc}], G^{lc}]G^{ia}). \end{aligned} \tag{F8}$$

Diagrams D_2 UV:

$$\begin{aligned} iT_{D_2}^{ba^{\mathrm{UV}}}(\text{no-pole}) &= -i\frac{\lambda_\epsilon}{(4\pi)^2}\left(\frac{\mathring{g}_A}{F_\pi}\right)^4\frac{1}{3}k_1^i k_2^j\sum_{n,n',n''}(G^{jb}\mathcal{P}_n G^{lc}\mathcal{P}_{n''}G^{ia}\mathcal{P}_{n'}G^{lc}(k_1^0+2p_1^0+\delta m_n-\delta m_{n'}-2\delta m_{n''}) \\ &\quad + G^{lc}\mathcal{P}_{n'}G^{jb}\mathcal{P}_{n''}G^{lc}\mathcal{P}_n G^{ia}(k_2^0+2p_2^0+\delta m_n-\delta m_{n'}-2\delta m_{n''})) \\ &= -i\frac{\lambda_\epsilon}{(4\pi)^2}\left(\frac{\mathring{g}_A}{F_\pi}\right)^4\frac{1}{3}k_1^i k_2^j(k_1^0 G^{jb}G^{lc}G^{ia}G^{lc}+k_2^0 G^{lc}G^{jb}G^{lc}G^{ia} \\ &\quad - 2G^{jb}G^{lc}G^{ia}[\delta\hat{m},G^{lc}]+G^{jb}[\delta\hat{m},G^{lc}]G^{ia}G^{lc}-G^{jb}G^{lc}[\delta\hat{m},G^{ia}]G^{lc} \\ &\quad + 2[\delta\hat{m},G^{lc}]G^{jb}G^{lc}G^{ia}+G^{lc}[\delta\hat{m},G^{jb}]G^{lc}G^{ia}-G^{lc}G^{jb}[\delta\hat{m},G^{lc}]G^{ia}) \end{aligned} \tag{F9}$$

Diagrams D_4 UV:

$$\begin{aligned} iT_{D_4}^{ba^{\mathrm{UV}}} &= i\frac{\lambda_\epsilon}{(4\pi)^2}\left(\frac{\mathring{g}_A}{F_\pi}\right)^4\frac{1}{3}k_1^i k_2^j(k_1^0+k_2^0+3p_1^0+3p_2^0-2\delta m_n-2\delta m_{n'}-2\delta m_{n''})G^{lc}\mathcal{P}_{n''}G^{jb}\mathcal{P}_{n'}G^{ia}\mathcal{P}_n G^{lc} \\ &= i\frac{\lambda_\epsilon}{(4\pi)^2}\left(\frac{\mathring{g}_A}{F_\pi}\right)^4\frac{1}{3}k_1^i k_2^j((k_1^0+k_2^0)G^{lc}G^{jb}G^{ia}G^{lc}+3[\delta\hat{m},G^{lc}]G^{jb}G^{ia}G^{lc} \\ &\quad - 3G^{lc}G^{jb}G^{ia}[\delta\hat{m},G^{lc}]+G^{lc}[\delta\hat{m},G^{jb}]G^{ia}G^{lc}-G^{lc}G^{jb}[\delta\hat{m},G^{ia}]G^{lc}). \end{aligned} \tag{F10}$$

The added UV divergencies of the no-pole terms of the diagrams D_1, D_2, and D_4 give

$$\begin{aligned} iT^{ba^{\mathrm{UV}}}(\text{no-pole})(\mathring{g}_A^4) &= i\frac{\lambda_\epsilon}{(4\pi)^2}\left(\frac{\mathring{g}_A}{F_\pi}\right)^4\frac{1}{3}k_1^i k_2^j(-(k_1^0+k_2^0)[G^{lc},G^{jb}][G^{lc},G^{ia}] \\ &\quad + 2\frac{C_{\mathrm{HF}}}{N_c}([G^{jb},[\delta\hat{m},G^{lc}]][G^{lc},G^{ia}]-[G^{lc},G^{jb}][G^{ia},[\delta\hat{m},G^{lc}]])). \end{aligned} \tag{F11}$$

b. Projection of UV divergence onto bases of SF operators

To the diagrams D_1 through D_4, the crossed diagrams must be added, which are obtained by the prescription $k_1 \leftrightarrow -k_2$, and $a \leftrightarrow b$. With this, the sum of the no-pole terms proportional to $\mathring{g}_A^4$ gives the UV divergence in terms of bases operators in Table IV:

$$\begin{aligned} iT^{ba^{\mathrm{UV}}}_{\text{no-pole}}(\mathring{g}_A^4) &= i\frac{\lambda_\epsilon}{(4\pi)^2}\left(\frac{\mathring{g}_A}{F_\pi}\right)^4\frac{1}{6}k_1^i k_2^j\left(\frac{i}{8}(k_1^0+k_2^0)(\delta^{ij}\epsilon^{bac}I^c+\delta^{ab}\epsilon^{jik}S^k)\right. \\ &\quad \left. + \frac{C_{\mathrm{HF}}}{N_c}(\delta^{ab}S^iS^j|_{J=2}+\delta^{ij}I^aI^b|_{I=2}-\frac{1}{2}\epsilon^{jik}\epsilon^{bac}(N_c(N_c+2)G^{kc}-3S^kI^c)-3G^{jb}G^{ia}|_{J=I=2})\right), \end{aligned} \tag{F12}$$

obtained from Eq. (F11) by making use of the relations

$$\begin{aligned} [G^{lc},G^{jb}][G^{lc},G^{ia}] &= -\frac{1}{16}\left(\frac{4}{3}\delta^{ij}\delta^{ab}\hat{S}^2+\frac{i}{2}\delta^{ab}\epsilon^{jik}S^k+\frac{i}{2}\delta^{ij}\epsilon^{abc}I^c+2\epsilon^{jik}\epsilon^{abc}S^kI^c\right. \\ &\quad \left. -\delta^{ab}S^iS^j|_{J=2}-\delta^{ij}I^aI^b|_{I=2}\right), \\ [G^{jb},[\delta\hat{m},G^{lc}]][G^{lc},G^{ia}]-[G^{lc},G^{jb}][G^{ia},[\delta\hat{m},G^{lc}]] &= \frac{C_{\mathrm{HF}}}{N_c}\left(\frac{i}{48}(3N_c(N_c+4)+6-28\hat{S}^2)(\delta^{ab}\epsilon^{jik}S^k+\delta^{ij}\epsilon^{bac}I^c)\right) \\ &\quad -\frac{1}{8}\epsilon^{jik}\epsilon^{bac}(N_c(N_c+2)G^{kc}-3S^kI^c)+\frac{1}{4}(\delta^{ab}S^iS^j|_{J=2}+\delta^{ij}I^aI^b|_{I=2}) \\ &\quad +\frac{i}{2}(\epsilon^{jik}S^kI^aI^b|_{I=2}+\epsilon^{bac}I^cS^iS^j|_{J=2})-3G^{jb}G^{ia}|_{J=I=2}\Big). \end{aligned} \tag{F13}$$

These UV divergencies give contributions that are at most $\mathcal{O}(N_c^0)$, and thus consistent with the $1/N_c$ expansion of the scattering amplitudes. They are also independent of M_π.

2. Diagrams $\propto \mathring{g}_A^2$

The diagrams $D_{6,7,8}$ vanish identically.

Diagrams D_5:

These diagrams give only single-pole contributions, correcting the π-baryon coupling, and thus are finally included in the pole contributions Eq. (15),

$$iT^{ba}_{D_5} = -i\left(\frac{\mathring{g}_A}{F_\pi^2}\right)^2 \frac{2}{3} k_1^i k_2^j \Delta(M_\pi) \sum_n G^{jb} \mathcal{P}_n G^{ia} \frac{1}{p_1^0 + k_1^0 - \delta m_n} \tag{F14}$$

where:

$$\Delta(M_\pi) = \int \widetilde{d^d k} \frac{i}{k^2 - M_\pi^2} = -\frac{M_p i^2}{(4\pi)^2}\left(\lambda_\epsilon - \log\frac{M_\pi^2}{\mu^2}\right) \tag{F15}$$

Diagrams D_9:

$$iT^{ba}_{D_9} = \left(\frac{\mathring{g}_A}{F_\pi^2}\right)^2 \frac{1}{6} \sum_n G^{kc} \mathcal{P}_n G^{kd} (\delta^{ac}\delta^{bd} + \delta^{ad}\delta^{bc} - 2\delta^{ab}\delta^{cd})(\mathcal{I}(\delta m_n - p_1^0, M_\pi) + \mathcal{I}(\delta m_n - p_2^0, M_\pi)). \tag{F16}$$

Diagram D_{10}:

This diagram is more compactly expressed in terms of the integrals defined earlier in Eqs. (E5) and (E6), and reads

$$\begin{aligned}
iT^{ba}_{D_{10}} = -i\left(\frac{\mathring{g}_A}{F_\pi^2}\right)^2 \frac{1}{3} \sum_n G^{ld} \mathcal{P}_n G^{jc} \frac{1}{(4\pi)^{d/2}} \Bigg(& \frac{1}{2}\delta^{jl}(\delta^{ac}\delta^{bd} + \delta^{ad}\delta^{bc} - 2\delta^{ab}\delta^{cd}) \\
& \times \Gamma\left(1 - \frac{d}{2}\right)\left(J\left(0, 1 - \frac{d}{2}, C_0^+, 1, \lambda_0^+\right) + J\left(0, 1 - \frac{d}{2}, C_0^-, 1, \lambda_0^-\right)\right) \\
& + 6\int_0^1 d\alpha \Bigg(\left((t - M_\pi^2)\delta^{ab}\delta^{cd} + \frac{1}{2}(2M_\pi^2 - t)(\delta^{ac}\delta^{bd} + \delta^{ad}\delta^{bc})\right) \\
& \times \left(\Gamma\left(3 - \frac{d}{2}\right) J\left(0, 3 - \frac{d}{2}, C_0^1, 1, \lambda_0^1\right) - \frac{1}{2}\delta^{jl}\Gamma\left(2 - \frac{d}{2}\right) J\left(0, 2 - \frac{d}{2}, C_0^1, 1, \lambda_0^1\right)\right) \\
& + (\delta^{ac}\delta^{bd} - \delta^{ad}\delta^{bc})\left(\frac{1}{2}(\alpha q^l (k_1 + k_2)^j + (\alpha - 1) q^j (k_1 + k_2)^l)\Gamma\left(2 - \frac{d}{2}\right) J\left(0, 2 - \frac{d}{2}, C_0^1, 1, \lambda_0^1\right)\right. \\
& + \alpha(1 - \alpha) q^j q^l (k_1^0 + k_2^0)\Gamma\left(3 - \frac{d}{2}\right) J\left(1, 3 - \frac{d}{2}, C_0^1, 1, \lambda_0^1\right) \\
& \left. - \frac{1}{2}\delta^{jl}(k_1^0 + k_2^0)\Gamma\left(2 - \frac{d}{2}\right) J\left(1, 2 - \frac{d}{2}, C_0^1, 1, \lambda_0^1\right)\right)\Bigg)\Bigg)
\end{aligned} \tag{F17}$$

where

$$\begin{aligned}
& d = 4 - 2\epsilon, \qquad q = k_1 - k_2, \qquad t = q^2 \\
& C_0^\pm = M_\pi^2 - \lambda_0^\pm, \qquad \lambda_0^\pm = \frac{1}{2}(p_1^0 + p_2^0 \pm q^0) - \delta m_n \\
& C_0^1 = M_\pi^2 + \alpha(\alpha - 1) q^2 - \lambda_0^1, \qquad \lambda_0^1 = \frac{1}{2}(p_1^0 + p_2^0) + \left(\frac{1}{2} - \alpha\right) q^0 - \delta m_n.
\end{aligned} \tag{F18}$$

Diagram D_{11}:

$$iT^{ba}_{D_{11}} = i\left(\frac{\mathring{g}_A}{F_\pi^2}\right)^2 \sum_{n,n'} G^{kc}\mathcal{P}_{n'}\left(-\frac{1}{2}(k_1^0+k_2^0)\epsilon^{bac}I^c + 2ic_1N_c\frac{M_\pi^2}{\Lambda}\delta^{ab}\right)\mathcal{P}_n G^{kd} \times \frac{1}{p_2^0-p_1^0-\delta m_{n'}+\delta m_n}(\mathcal{I}(\delta m_{n'}-p_2^0,M_\pi)-\mathcal{I}(\delta m_n-p_1^0,M_\pi)). \tag{F19}$$

Diagram D_{12}:

$$iT^{ba}_{D_{12}} = \frac{1}{2}\frac{1}{F_\pi^2}\left\{\frac{1}{2}(k_1^0+k_2^0)\epsilon^{bac}I^c + 2ic_1N_c\frac{M_\pi^2}{\Lambda}\delta^{ab}, \delta\hat{Z}\right\} \tag{F20}$$

where δZ is evaluated on-shell for the in and out baryons, which in this case have the same spin.

a. UV divergencies of the no-pole terms

The UV divergent pieces of no-pole terms of the diagrams proportional to $\mathring{g}_A^2$, evaluated for the external baryons on mass shell are as follows:

Diagram D_9 UV:

$$iT^{ba^{\rm UV}}_{D_9} = -i\frac{\lambda_\epsilon}{(4\pi)^2}\left(\frac{\mathring{g}_A}{F_\pi^2}\right)^2\sum_n G^{ie}\mathcal{P}_n G^{ic}(\delta^{ae}\delta^{bc}+\delta^{ac}\delta^{be}-2\delta^{ab}\delta^{ce}) \times\frac{1}{16}(3M_\pi^2((p_1^0-\delta m_n)+(p_2^0-\delta m_n))-2((p_1^0-\delta m_n)^3+(p_2^0-\delta m_n)^3)). \tag{F21}$$

This diagram projects onto $J=0, I=0,\ 2$, implying that $p_1^0=p_2^0=\delta m_{\rm in}$, and yielding

$$\begin{aligned} iT^{ba^{\rm UV}}_{D_9}(J=I=0) &= i\frac{\lambda_\epsilon}{(4\pi)^2}\left(\frac{\mathring{g}_A}{F_\pi^2}\right)^2\delta^{ab}\frac{2}{9}\frac{C_{\rm HF}}{N_c}\left(M_\pi^2\left(5\hat{S}^2-\frac{3}{4}N_c(N_c+4)\right)\right. \\ &\quad\left.+\left(\frac{C_{\rm HF}}{N_c}\right)^2\left(\frac{2}{3}(5N_c(N_c+4)-24)\hat{S}^2+2N_c(N_c+4)-\frac{56\hat{S}^4}{3}\right)\right), \\ iT^{ba^{\rm UV}}_{D_9}(J=0,I=2) &= i\frac{\lambda_\epsilon}{(4\pi)^2}\left(\frac{\mathring{g}_A}{F_\pi^2}\right)^2 I^aI^b|_{I=2}\frac{1}{3}\frac{C_{\rm HF}}{N_c}\left(M_\pi^2+\left(\frac{C_{\rm HF}}{N_c}\right)^2\left(\frac{2}{3}N_c(N_c+4)-\frac{16\hat{S}^2}{3}\right)\right). \end{aligned} \tag{F22}$$

Diagram D_{10} UV: Upon projecting the diagram onto t-channel (J,I), the corresponding UV divergent amplitudes are the following:

$$\begin{aligned} iT^{ba^{\rm UV}}_{D_{10}}(J=I=0) &= \frac{i}{54}\frac{\lambda_\epsilon}{(4\pi)^2}\left(\frac{\mathring{g}_A}{F_\pi^2}\right)^2\sum_n G^{ic}\mathcal{P}_n G^{ic}\delta^{ab}(p_1^0+p_2^0-2\delta m_n) \\ &\quad\times(6(k_1^0-k_2^0)^2-21M_\pi^2+2((p_1^0+p_2^0-2\delta m_n)^2+9t)) \\ &= i\frac{\lambda_\epsilon}{(4\pi)^2}\left(\frac{\mathring{g}_A}{F_\pi^2}\right)^2\frac{1}{9}\delta^{ab}\frac{C_{\rm HF}}{N_c}\left(-\frac{3}{8}N_c(N_c+4)(5M_\pi^2-12k_1\cdot k_2)\right. \\ &\quad+\left(\frac{C_{\rm HF}}{N_c}\right)^2\left(-\frac{4}{3}(5N_c(N_c+4)-24)\hat{S}^2-4N_c(N_c+4)+\frac{112}{3}\hat{S}^4\right) \\ &\quad\left.+\hat{S}^2\left(\frac{25}{2}M_\pi^2-30k_1\cdot k_2\right)\right), \end{aligned} \tag{F23}$$

$$iT_{D_{10}}^{ba^{\mathrm{UV}}}(J=0,I=1) = -\frac{i}{18}\frac{\lambda_\epsilon}{(4\pi)^2}\left(\frac{\mathring{g}_A}{F_\pi^2}\right)^2\sum_n G^{ie}\mathcal{P}_n G^{ic}\frac{1}{2}(\delta^{ae}\delta^{bc}-\delta^{ac}\delta^{be})$$
$$\times((k_1^0+k_2^0)(3((k_1^0-k_2^0)^2-6M_\pi^2+3(p_1^0+p_2^0-2\delta m_n)^2+t)-2(\vec{k}1-\vec{k}2)^2)+2(k_1^0-k_2^0)(\vec{k}_1^2-\vec{k}_2^2))$$
$$=\frac{\lambda_\epsilon}{(4\pi)^2}\left(\frac{\mathring{g}_A}{F_\pi^2}\right)^2\frac{1}{4}\epsilon^{bac}I^c(k_1^0+k_2^0)\left(\frac{1}{6}(3k_1\cdot k_2+(\vec{k}_1-\vec{k}_2)^2+6M_\pi^2)\right.$$
$$\left.+\left(\frac{C_{\mathrm{HF}}}{N_c}\right)^2(3N_c(N_c+4)-20\hat{S}^2)\right), \tag{F24}$$

$$iT_{D_{10}}^{ba^{\mathrm{UV}}}(J=0,I=2) = -\frac{i}{18}\frac{\lambda_\epsilon}{(4\pi)^2}\left(\frac{\mathring{g}_A}{F_\pi^2}\right)^2\sum_n G^{ie}\mathcal{P}_n G^{ic}\frac{1}{2}\left(\delta^{ae}\delta^{bc}+\delta^{be}\delta^{ac}-\frac{2}{3}\delta^{ab}\delta^{ce}\right)$$
$$\times(p_1^0+p_2^0-2\delta m_n)(3(k_1^0-k_2^0)^2-24M_\pi^2+(p_1^0+p_2^0-2\delta m_n)^2+9t)$$
$$=i\frac{\lambda_\epsilon}{(4\pi)^2}\left(\frac{\mathring{g}_A}{F_\pi^2}\right)^2 I^aI^b|_{I=2}\frac{1}{9}\frac{C_{\mathrm{HF}}}{N_c}\left(-3(3k_1\cdot k_2+M_\pi^2)+\left(\frac{C_{\mathrm{HF}}}{N_c}\right)^2(16\hat{S}^2-2N_c(N_c+4))\right), \tag{F25}$$

$$iT_{D_{10}}^{ba^{\mathrm{UV}}}(J=I=1) = -i\frac{\lambda_\epsilon}{(4\pi)^2}\left(\frac{\mathring{g}_A}{F_\pi^2}\right)^2\sum_n G^{le}\mathcal{P}_n G^{jc}\frac{1}{2}(\delta^{ae}\delta^{bc}-\delta^{ac}\delta^{be})(p_1^0+p_2^0-2\delta m_n)((\vec{k}_1^j-\vec{k}_2^j)(\vec{k}_1^l+\vec{k}_2^l))|_{J=1}$$
$$=i\frac{\lambda_\epsilon}{(4\pi)^2}\left(\frac{\mathring{g}_A}{F_\pi^2}\right)^2\epsilon^{bac}\epsilon^{jil}\frac{C_{\mathrm{HF}}}{N_c}\frac{1}{2}k_1^ik_2^j(G^{lc}(N_c+2)-3I^cS^l). \tag{F26}$$

Diagram D_{11} UV:

$$iT_{D_{11}}^{ba^{\mathrm{UV}}} = -\frac{\lambda_\epsilon}{(4\pi)^2}\left(\frac{\mathring{g}_A}{F_\pi^2}\right)^2\frac{1}{6}\sum_n(3M_\pi^2-2((p_1^0-\delta m_n)(p_2^0-\delta m_n)+(p_1^0-\delta m_n)^2+(p_2^0-\delta m_n)^2))$$
$$\times\left(\epsilon^{abc}(k_1^0+k_2^0)G^{ie}\mathcal{P}_nI^cG^{ie}-4i\delta^{ab}c_1N_c\frac{M_\pi^2}{\Lambda}G^{ie}\mathcal{P}_nG^{ie}\right), \tag{F27}$$

$$iT_{D_{11}}^{ba^{\mathrm{UV}}}(J=I=0) = i\frac{\lambda_\epsilon}{(4\pi)^2}\left(\frac{\mathring{g}_A}{F_\pi^2}\right)^2\delta^{ab}\mathrm{c}1N_c\frac{M_\pi^2}{\Lambda}\left(M_\pi^2\left(\frac{3}{8}N_c(N_c+4)-\hat{S}^2\right)\right.$$
$$\left.+\left(\frac{C_{\mathrm{HF}}}{N_c}\right)^2(-2(N_c-2)(N_c+6)\hat{S}^2-3N_c(N_c+4)+8\hat{S}^4)\right),$$
$$iT_{D_{11}}^{ba^{\mathrm{UV}}}(J=0,I=1) = \frac{\lambda_\epsilon}{(4\pi)^2}\left(\frac{\mathring{g}_A}{F_\pi^2}\right)^2\frac{1}{4}\epsilon^{bac}I^c(k_1^0+k_2^0)\left(M_\pi^2\left(\frac{3}{8}(N_c(N_c+4)-4)-\hat{S}^2\right)\right.$$
$$\left.+\left(\frac{C_{\mathrm{HF}}}{N_c}\right)^2\left(-2N_c(N_c+4)(\hat{S}^2+3)+4\hat{S}^2(2\hat{S}^2+11)\right)\right). \tag{F28}$$

Diagram D_{12} UV:

$$iT_{D_{12}}^{ba^{\mathrm{UV}}} = \frac{\lambda_\epsilon}{(4\pi)^2}\left(\frac{\mathring{g}_A}{F_\pi^2}\right)^2\frac{1}{2}\sum_n G^{id}\mathcal{P}_nG^{id}(M_\pi^2-(p_1^0-\delta m_n)^2-(p_2^0-\delta m_n)^2)$$
$$\times\left(-4i\delta^{ab}c_1N_c\frac{M_\pi^2}{\Lambda}+\epsilon^{abc}I^c(k_1^0+k_2^0)\right), \tag{F29}$$

$$
\begin{aligned}
iT^{ba^{\mathrm{UV}}}_{D_{12}}(J=I=0) &= i\frac{\lambda_\epsilon}{(4\pi)^2}\left(\frac{\mathring{g}_A}{F_\pi^2}\right)^2\delta^{ab}\mathrm{c1}N_c\frac{M_\pi^2}{\Lambda}\left(M_\pi^2\left(\hat{S}^2-\frac{3}{8}N_c(N_c+4)\right)\right.\\
&\left.+\left(\frac{C_{\mathrm{HF}}}{N_c}\right)^2(2(N_c-2)(N_c+6)\hat{S}^2+3N_c(N_c+4)-8\hat{S}^4)\right),\\
iT^{ba^{\mathrm{UV}}}_{D_{12}}(J=0,I=1) &= \frac{\lambda_\epsilon}{(4\pi)^2}\left(\frac{\mathring{g}_A}{F_\pi^2}\right)^2\frac{1}{4}\epsilon^{bac}I^c(k_1^0+k_2^0)\left(M_\pi^2\left(\hat{S}^2-\frac{3}{8}N_c(N_c+4)\right)\right.\\
&\left.+\left(\frac{C_{\mathrm{HF}}}{N_c}\right)^2(2(N_c-2)(N_c+6)\hat{S}^2+3N_c(N_c+4)-8\hat{S}^4)\right).
\end{aligned}
\tag{F30}
$$

Adding up the diagrams, the $\mathring{g}_A^2$ UV divergencies yield

$$
\begin{aligned}
iT^{ba^{\mathrm{UV}}}(\mathring{g}_A^2) &= i\frac{\lambda_\epsilon}{(4\pi)^2}\left(\frac{\mathring{g}_A}{F_\pi^2}\right)^2\frac{1}{4}\left(2\frac{C_{\mathrm{HF}}}{N_c}\epsilon^{bac}\epsilon^{jil}k_1^i k_2^j(G^{lc}(N_c+2)-3I^cS^l\right)\\
&+\frac{i}{2}\epsilon^{bac}I^c(k_1^0+k_2^0)\left(-k_1\cdot k_2-\frac{1}{3}(\vec{k}_1-\vec{k}_2)^2+M_\pi^2\right)\\
&+\frac{C_{\mathrm{HF}}}{N_c}\delta^{ab}\left(k_1\cdot k_2\left(2N_c(N_c+4)-\frac{40\hat{S}^2}{3}\right)+M_\pi^2\left(\hat{S}^2-\frac{3}{2}N_c(N_c+4)\right)\right)\\
&-4\frac{C_{\mathrm{HF}}}{N_c}I^aI^b|_{I=2}\,k_1\cdot k_2\Big).
\end{aligned}
\tag{F31}
$$

In the $J=0$ terms $k_1^0=k_2^0$, which in the term $(J=0,I=1)$ gives the simplification $(-k_1\cdot k_2-\frac{1}{3}(\vec{k}_1-\vec{k}_2)^2+M_\pi^2)\to\frac{1}{6}t$.

3. Diagrams $\propto \mathring{g}_A^0$

In these diagrams the baryon flowing through it has a fixed spin, thus in the CM frame $k_1^0=k_2^0$, and each diagram satisfies large N_c consistency. The results are as follows:

Diagram D_{13}:

$$
iT^{ba}_{D_{13}} = -\frac{1}{(4\pi)^2}\frac{5}{F_\pi^4}M_\pi^2\left(\lambda_\epsilon+1-\log\frac{M_\pi^2}{\mu^2}\right)\left(\frac{1}{24}\epsilon^{bac}I^c(k_1^0+k_2^0)+\frac{i}{3}\delta^{ab}c_1N_c\frac{M_\pi^2}{\Lambda}\right).
\tag{F32}
$$

Diagram D_{14}:

$$
\begin{aligned}
iT^{ba}_{D_{14}} &= \frac{1}{F_\pi^4}\frac{1}{(4\pi)^2}\left(ic_1N_c\frac{M_\pi^2}{\Lambda}\delta^{ab}\left(\left(\frac{7}{3}M_\pi^2-2t\right)\left(\lambda_\epsilon-\log\frac{M_\pi^2}{\mu^2}\right)+\frac{10M_\pi^2}{3}-4t-2\sqrt{1-\frac{4M_\pi^2}{t}}(M_\pi^2-2t)\arctan\frac{\sqrt{t}}{\sqrt{-4M_\pi^2+t}}\right)\right.\\
&\left.+2\epsilon^{bac}I^c(k_1^0+k_2^0)\left(\left(M_\pi^2-\frac{t}{6}\right)\left(\lambda_\epsilon-\log\frac{M_\pi^2}{\mu^2}\right)+\frac{7}{3}M_\pi^2-4t+\frac{1}{3}(-4M_\pi^2+t)^{3/2}\arctan\frac{\sqrt{t}}{\sqrt{-4M_\pi^2+t}}\right)\right).
\end{aligned}
\tag{F33}
$$

Diagram D_{15}:

$$
\begin{aligned}
iT^{ba}_{D_{15}} &= -\frac{1}{F_\pi^4}\left(\frac{i}{4}\epsilon^{bac}I^c\left(\frac{1}{2}\Gamma\left(1-\frac{d}{2}\right)J\left(0,1-\frac{d}{2},C_0,1,\lambda_0\right)\right.\right.\\
&-\Gamma\left(2-\frac{d}{2}\right)\left(k_1^0k_2^0J\left(0,2-\frac{d}{2},C_0,1,\lambda_0\right)+(k_1^0+k_2^0)J\left(1,2-\frac{d}{2},C_0,1,\lambda_0\right)\right.\\
&\left.\left.+J\left(2,2-\frac{d}{2},C_0,1,\lambda_0\right)+4c_1N_c\frac{M_\pi^2}{\Lambda}\left((k_1^0+k_2^0)J\left(0,2-\frac{d}{2},C_0,1,\lambda_0\right)+2J\left(1,2-\frac{d}{2},C_0,1,\lambda_0\right)\right)\right)\right)\\
&-4\delta^{ab}c_1^2N_c^2\frac{M_\pi^4}{\Lambda^2}\Gamma\left(2-\frac{d}{2}\right)J\left(0,2-\frac{d}{2},C_0,1,\lambda_0\right)\Big),
\end{aligned}
\tag{F34}
$$

where $C_0 = M_\pi^2 - \lambda_0^2$ and $\lambda_0 = k_1^0 = k_2^0$. Adding the crossed diagram and, in order to simplify the result, using explicitly that $k_1^0 = k_2^0$ in the CM frame, yields

$$\begin{aligned} iT^{ba}_{D_{15}+\text{crossed}} = \frac{1}{(4\pi)^2}\frac{1}{F_\pi^4}\Bigg(&-i\delta^{ab}8\pi\sqrt{M_\pi^2 - k_1^{0^2}}\left(\frac{1}{3}k_1^0\hat{S}^2 + 2c_1^2N_c^2\frac{M_\pi^4}{\Lambda^2}\right) \\ &+ \epsilon^{bac}I^c k_1^0\Bigg(\left(\frac{3}{4}M_\pi^2 - 2k_1^{0^2}\right)\left(\lambda_\epsilon + 1 - \log\frac{M_\pi^2}{\mu^2}\right) - 2k_1^{0^2} \\ &+ 4\sqrt{M_\pi^2 - k_1^{0^2}}\left(-4\pi c_1 N_c\frac{M_\pi^2}{\Lambda} + k_1^0\arctan\frac{k_1^0}{\sqrt{M_\pi^2 - k_1^{0^2}}}\right)\Bigg) + i4\pi k_1^{0^2}\sqrt{M_\pi^2 - k_1^{0^2}}I^aI^b|_{I=2}\Bigg). \end{aligned} \tag{F35}$$

a. UV divergencies

Diagram D_{13} UV:

$$iT^{ba^{\text{UV}}}_{D_{13}} = -\frac{\lambda_\epsilon}{(4\pi)^2}\frac{5}{F_\pi^4}M_\pi^2\left(\frac{1}{32}\epsilon^{bac}I^c(k_1^0 + k_2^0) + \frac{i}{3}\delta^{ab}c_1N_c\frac{M_\pi^2}{\Lambda}\right). \tag{F36}$$

Diagram D_{14} UV:

$$iT^{ba^{\text{UV}}}_{D_{14}} = \frac{\lambda_\epsilon}{(4\pi)^2}\frac{1}{F_\pi^4}\frac{1}{12}\left(4ic_1N_c\frac{M_\pi^2}{\Lambda}\delta^{ab}(7M_\pi^2 - 6t) + \epsilon^{bac}I^c(k_1^0 + k_2^0)(6M_\pi^2 - t)\right). \tag{F37}$$

Diagram D_{15} UV:
Adding the crossed diagram to D_{15} yields

$$iT^{ba^{\text{UV}}}_{D_{15}+\text{crossed}} = -\frac{\lambda_\epsilon}{(4\pi)^2}\frac{1}{F_\pi^4}\epsilon^{bac}I^c\frac{1}{4}(k_1^0 + k_2^0)\left((k_1^0 + k_2^0)^2 - \frac{3}{2}M_\pi^2\right). \tag{F38}$$

Adding up the diagrams, the UV divergences proportional to $\mathring{g}_A^0$ become

$$iT^{ba^{\text{UV}}}(\mathring{g}_A^0) = \frac{\lambda_\epsilon}{(4\pi)^2}\frac{1}{12F_\pi^4}\left(i\delta^{ab}8c_1N_c\frac{M_\pi^2}{\Lambda}(M_\pi^2 - 3t) + \epsilon^{bac}I^c(k_1^0 + k_2^0)(3(k_1^0 + k_2^0)^2 - 8M_\pi^2 + t)\right). \tag{F39}$$

4. β functions

The β functions corresponding to the LECs of the CT Lagrangians equations (D5)–(D7) are given in Table VII. The definition of the β function for a given LEC X is

$$X \equiv X(\mu) + \beta_X\frac{\lambda_\epsilon}{(4\pi)^2}, \tag{F40}$$

where $X(\mu)$ is the renormalized LEC at the renormalization scale μ. For the Lagrangian equation (D8) the β functions obviously vanish.

5. Counterterm contributions to the amplitudes

The contributions from the Lagrangians equations (D5)–(D8) to the scattering amplitudes for definite t-channel (J, I) are the following:

TABLE VII. β functions of the NLO and NNLO Lagrangians equations (D5)–(D7).

LEC	$\beta_{f_{JI}}/(\frac{\mathring{g}_A^4}{F_\pi^2})$	LEC	$\beta_{g_{JI}}/(\Lambda\frac{\mathring{g}_A^2}{F_\pi^2})$	LEC	$\beta_{h_{JI}}/(\frac{\Lambda^2}{F_\pi^2})$
$f_{10}^{(1)}$	$\frac{\Lambda^2}{96}$	$g_{00}^{(1)}$	$-\frac{3}{32}(N_c+4)C_{\rm HF}$	$h_{00}^{(1)}+h_{00}^{(2)}$	$-\frac{5}{24}c_1$
$f_{01}^{(1)}$	$\frac{\Lambda^2}{96}$	$g_{00}^{(2)}$	$\frac{1}{16}C_{\rm HF}$	$h_{00}^{(3)}$	$-\frac{1}{2}c_1$
$f_{11}^{(1)}$	$\frac{N_c+2}{12N_c}\Lambda C_{\rm HF}$	$g_{00}^{(3)}$	$-\frac{1}{4}(N_c+4)C_{\rm HF}$	$h_{01}^{(1)}$	$\frac{1}{2}$
$f_{11}^{(2)}$	$-\frac{1}{4}\Lambda C_{\rm HF}$	$g_{00}^{(4)}$	$\frac{5}{3}C_{\rm HF}$	$h_{01}^{(2)}$	$\frac{1}{12}$
f_{02}	$-\frac{1}{6}\Lambda C_{\rm HF}$	$g_{01}^{(1)}$	$-\frac{1}{48}\Lambda$	$h_{01}^{(3)}$	$\frac{1}{4}$
f_{20}	$-\frac{1}{6}\Lambda C_{\rm HF}$	$g_{01}^{(2)}$	$-\frac{1}{48}\Lambda$		
f_{22}	$\Lambda C_{\rm HF}$	$g_{02}^{(1)}$	$\frac{1}{2N_c}C_{\rm HF}$		
		$g_{11}^{(1)}$	$\frac{N_c+2}{4N_c}C_{\rm HF}$		
		$g_{11}^{(2)}$	$-\frac{3}{4}C_{\rm HF}$		

$$iT^{ba}_{\rm CT}(J=I=0)=i2\frac{\delta^{ab}}{F_\pi^2}\left(-2\frac{g_{00}^{(1)}}{\Lambda}M_\pi^2-2\frac{g_{00}^{(2)}}{\Lambda}M_\pi^2\frac{\hat{S}^2}{N_c}-8\frac{(h_{00}^{(1)}+h_{00}^{(2)})}{\Lambda^3}N_cM_\pi^4+\frac{g_{00}^{(3)}}{\Lambda}k_1\cdot k_2\right.$$
$$\left.+\frac{g_{00}^{(4)}}{\Lambda}k_1\cdot k_2\frac{\hat{S}^2}{N_c}+2\frac{h_{00}^{(3)}}{\Lambda^3}N_cM_\pi^2k_1\cdot k_2+\frac{1}{2}\frac{l_{00}^{(1)}}{\Lambda^2}(k_1^ik_2^0+k_1^0k_2^i)(p_1^i+p_2^i)-2\frac{l_{00}^{(2)}}{\Lambda^2}M_\pi^2(p_1^0+p_2^0)\right),\quad\text{(F41)}$$

$$iT^{ba}_{\rm CT}(J=0,I=1)=\frac{1}{F_\pi^2}\epsilon^{abc}I^c\left(2\frac{\tilde{f}_{01}^{(1)}}{\Lambda^2}k_1\cdot k_2(k_1^0+k_2^0)+2\frac{\tilde{g}_{01}^{(1)}}{\Lambda^2}M_\pi^2(k_1^0+k_2^0)-\frac{l_{01}^{(1)}}{2m_0}(\vec{k}_1+\vec{k}_2)\cdot(\vec{p}_1+\vec{p}_2)\right.$$
$$\left.-\frac{l_{01}^{(2)}}{\Lambda^2}(k_1^i+k_2^i)(k_1^ik_2^0+k_1^0k_2^i)+\frac{l_{01}^{(3)}}{\Lambda^2}(k_1^0\vec{k}_2^2+k_2^0\vec{k}_1^2-\vec{k}_1\cdot\vec{k}_2(k_1^0+k_2^0))\right),\quad\text{(F42)}$$

$$iT^{ba}_{\rm CT}(J=1,I=0)=\frac{\epsilon^{ijk}S^k}{F_\pi^2}\left(-2\frac{f_{10}^{(1)}}{\Lambda^2}(k_1^0+k_2^0)k_1^ik_2^j-\frac{l_{10}^{(1)}}{\Lambda^2}(k_1^j+k_2^j)(k_1^ik_2^0-k_2^ik_1^0)+\frac{l_{10}^{(2)}}{\Lambda^2}(k_1^j-k_2^j)(k_1^ik_2^0+k_2^ik_1^0)\right),\quad\text{(F43)}$$

$$iT^{ba}_{\rm CT}(J=I=1)=i\frac{\epsilon^{ijk}\epsilon^{abc}}{F_\pi^2}\left(2\frac{\tilde{f}_{11}^{(1)}}{\Lambda}k_1^ik_2^jG^{kc}+2\frac{\tilde{f}_{11}^{(2)}}{\Lambda}\frac{1}{N_c}k_1^ik_2^jS^kI^c+\frac{l_{11}^{(1)}}{\Lambda^2}(k_1^ik_2^0-k_2^ik_1^0)(p_1^j+p_2^j)G^{kc}+\frac{l_{11}^{(2)}}{\Lambda^2}2k_1^ik_2^j(p_1^0+p_2^0)G^{kc}\right).\quad\text{(F44)}$$

These contributions for the $\pi N\to\pi N$ amplitudes are significantly simplified. For matrix elements between nucleon states, the generator G^{ia} is replaced by $G^{ia}\to\frac{N_c+2}{3}S^iI^a$. In the CM frame, the CT amplitudes then become

$$iT^{ba}_{\rm CT}(J=I=0)=i\frac{1}{F_\pi^2}\delta^{ab}\left(\alpha_{00}^{(1)}\frac{M_\pi^2}{\Lambda}+\alpha_{00}^{(2)}N_c\frac{M_\pi^4}{\Lambda^3}+\alpha_{00}^{(3)}\frac{k_1\cdot k_2}{\Lambda}+\alpha_{00}^{(4)}N_c\frac{M_\pi^2k_1\cdot k_2}{\Lambda^3}+\alpha_{00}^{(5)}\frac{k^0}{\Lambda}(\vec{k}_1+\vec{k}_2)^2\right),$$
$$iT^{ba}_{\rm CT}(J=0,I=1)=\frac{1}{F_\pi^2}\epsilon^{bac}I^c\left(\alpha_{01}^{(1)}M_\pi^2\frac{k^0}{\Lambda^2}+\alpha_{01}^{(2)}\frac{k^0}{\Lambda^2}k_1\cdot k_2+\alpha_{01}^{(3)}\frac{1}{m_0}(\vec{k}_1+\vec{k}_2)^2+\alpha_{01}^{(4)}\frac{k^0}{\Lambda^2}(\vec{k}_1+\vec{k}_2)^2\right),$$
$$iT^{ba}_{\rm CT}(J=1,I=0)=\frac{1}{F_\pi^2}\epsilon^{jik}S^k\alpha_{10}^{(1)}\frac{k^0}{\Lambda^2}k_1^ik_2^j$$
$$iT^{ba}_{\rm CT}(J=I=1)=i\frac{1}{F_\pi^2}\epsilon^{bac}\epsilon^{jik}S^kI^ck_1^ik_2^j\left(\alpha_{11}^{(1)}\frac{N_c}{\Lambda}+\alpha_{11}^{(2)}\frac{k^0}{\Lambda^2}\right),\quad\text{(F45)}$$

TABLE VIII. Ranges of agreement with data of the different BChPT works that explicitly include the Δ.

2-body operators

n	$G^{ia}\mathcal{P}_n G^{ia}$	$\epsilon^{abc}G^{ib}\mathcal{P}_n G^{ia}$	$\epsilon^{ijk}\epsilon^{abc}G^{jb}\mathcal{P}_n G^{ia}$
N	$\frac{1}{16}(N_c+2)^2$	$-\frac{i}{12}I^c(N_c+2)^2$	$-\frac{1}{9}I^cS^k(N_c+2)^2$
Δ	$\frac{1}{8}(N_c-1)(N_c+5)$	$\frac{i}{12}I^c(N_c-1)(N_c+5)$	$-\frac{1}{18}I^cS^k(N_c-1)(N_c+5)$

3-body operators

n	$G^{ia}\mathcal{P}_n I^c G^{ia}$
N	$-\frac{1}{48}I^c(N_c+2)^2$
Δ	$\frac{5}{24}I^c(N_c-1)(N_c+5)$

4-body operators

n_1	n_2	n_3	$G^{ia}\mathcal{P}_{n_3}G^{kc}\mathcal{P}_{n_2}G^{kc}\mathcal{P}_{n_1}G^{ia}$	$\epsilon^{abc}G^{ib}\mathcal{P}_{n_3}G^{kd}\mathcal{P}_{n_2}G^{kd}\mathcal{P}_{n_1}G^{ia}$
N	N	N	$\frac{1}{256}(N_c+2)^4$	$-\frac{i}{192}I^c(N_c+2)^4$
N	Δ	N	$\frac{1}{128}(N_c-1)(N_c+2)^2(N_c+5)$	$-\frac{i}{96}I^c(N_c-1)(N_c+2)^2(N_c+5)$
Δ	N	Δ	$\frac{1}{256}(N_c-1)^2(N_c+5)^2$	$\frac{i}{384}I^c(N_c-1)^2(N_c+5)^2$
Δ	Δ	Δ	$\frac{1}{128}(N_c-1)(N_c+2)^2(N_c+5)$	$\frac{i}{192}I^c(N_c-1)(N_c+2)^2(N_c+5)$
Δ	Δ_5	Δ	$\frac{3}{256}(N_c-3)(N_c-1)(N_c+5)(N_c+7)$	$\frac{i}{128}I^c(N_c-3)(N_c-1)(N_c+5)(N_c+7)$

4-body operators

n_1	n_2	n_3	$G^{ia}\mathcal{P}_{n_3}G^{kd}\mathcal{P}_{n_2}G^{ia}\mathcal{P}_{n_1}G^{kd}$	$\epsilon^{ijk}\epsilon^{abc}G^{jb}\mathcal{P}_{n_3}G^{ld}\mathcal{P}_{n_2}G^{ld}\mathcal{P}_{n_1}G^{ia}$
N	N	N	$\frac{(N_c+2)^4}{2304}$	$-\frac{1}{144}I^cS^k(N_c+2)^4$
N	N	Δ	$\frac{1}{288}(N_c-1)(N_c+2)^2(N_c+5)$	0
N	Δ	N	$\frac{1}{288}(N_c-1)(N_c+2)^2(N_c+5)$	$-\frac{1}{72}I^cS^k(N_c-1)(N_c+2)^2(N_c+5)$
N	Δ	Δ	$\frac{5(N_c-1)(N_c+2)^2(N_c+5)}{1152}$	0
Δ	N	N	$\frac{1}{288}(N_c-1)(N_c+2)^2(N_c+5)$	0
Δ	N	Δ	$\frac{(N_c-1)^2(N_c+5)^2}{2304}$	$-\frac{1}{576}I^cS^k(N_c-1)^2(N_c+5)^2$
Δ	Δ	N	$\frac{5(N_c-1)(N_c+2)^2(N_c+5)}{1152}$	0
Δ	Δ	Δ	$\frac{1}{288}(N_c-1)(N_c+2)^2(N_c+5)$	$-\frac{1}{288}I^cS^k(N_c-1)(N_c+2)^2(N_c+5)$
Δ	Δ_5	Δ	$\frac{3}{256}(N_c-3)(N_c-1)(N_c+5)(N_c+7)$	$-\frac{1}{192}I^cS^k(N_c-3)(N_c-1)(N_c+5)(N_c+7)$

4-body operators

n_1	n_2	n_3	$\epsilon^{abc}G^{ib}\mathcal{P}_{n_3}G^{kd}\mathcal{P}_{n_2}G^{ia}\mathcal{P}_{n_1}G^{kd}$	$\epsilon^{ijk}\epsilon^{abc}G^{jb}\mathcal{P}_{n_3}G^{ld}\mathcal{P}_{n_2}G^{ia}\mathcal{P}_{n_1}G^{ld}$
N	N	N	$-\frac{i}{1728}I^c(N_c+2)^4$	$-\frac{1}{1296}I^cS^k(N_c+2)^4$
N	N	Δ	$\frac{i}{432}I^c(N_c-1)(N_c+2)^2(N_c+5)$	$-\frac{1}{648}I^cS^k(N_c-1)(N_c+2)^2(N_c+5)$
N	Δ	N	$-\frac{i}{216}I^c(N_c-1)(N_c+2)^2(N_c+5)$	$-\frac{1}{162}I^cS^k(N_c-1)(N_c+2)^2(N_c+5)$
N	Δ	Δ	$\frac{5i}{1728}I^c(N_c-1)(N_c+2)^2(N_c+5)$	$-\frac{5}{2592}I^cS^k(N_c-1)(N_c+2)^2(N_c+5)$
Δ	N	N	$-\frac{i}{216}I^c(N_c-1)(N_c+2)^2(N_c+5)$	$-\frac{1}{162}I^cS^k(N_c-1)(N_c+2)^2(N_c+5)$
Δ	N	Δ	$\frac{i}{3456}I^c(N_c-1)^2(N_c+5)^2$	$-\frac{1}{5184}I^cS^k(N_c-1)^2(N_c+5)^2$
Δ	Δ	N	$-\frac{5i}{864}I^c(N_c-1)(N_c+2)^2(N_c+5)$	$-\frac{5}{648}I^cS^k(N_c-1)(N_c+2)^2(N_c+5)$
Δ	Δ	Δ	$\frac{i}{432}I^c(N_c-1)(N_c+2)^2(N_c+5)$	$-\frac{1}{648}I^cS^k(N_c-1)(N_c+2)^2(N_c+5)$
Δ	Δ_5	Δ	$\frac{i}{128}I^c(N_c-3)(N_c-1)(N_c+5)(N_c+7)$	$-\frac{1}{192}I^cS^k(N_c-3)(N_c-1)(N_c+5)(N_c+7)$

4-body operators

n_1	n_2	n_3	$\epsilon^{ijk}\epsilon^{abc}G^{ld}\mathcal{P}_{n_3}G^{jb}\mathcal{P}_{n_2}G^{ia}\mathcal{P}_{n_1}G^{ld}$	$\epsilon^{abc}G^{ld}\mathcal{P}_{n_3}G^{ib}\mathcal{P}_{n_2}G^{ia}\mathcal{P}_{n_1}G^{ld}$
N	N	N	$-\frac{1}{1296}I^cS^k(N_c+2)^4$	$\frac{i}{576}I^c(N_c+2)^4$
N	N	Δ	$-\frac{1}{648}I^cS^k(N_c-1)(N_c+2)^2(N_c+5)$	0

(Table continued)

TABLE VIII. *(Continued)*

4-body operators				
n_1	n_2	n_3	$\epsilon^{ijk}\epsilon^{abc}G^{ld}\mathcal{P}_{n_3}G^{jb}\mathcal{P}_{n_2}G^{ia}\mathcal{P}_{n_1}G^{ld}$	$\epsilon^{abc}G^{ld}\mathcal{P}_{n_3}G^{ib}\mathcal{P}_{n_2}G^{ia}\mathcal{P}_{n_1}G^{ld}$
N	Δ	N	$-\frac{1}{2592}I^cS^k(N_c-1)(N_c+2)^2(N_c+5)$	$-\frac{i}{576}I^c(N_c-1)(N_c+2)^2(N_c+5)$
N	Δ	Δ	$-\frac{5}{648}I^cS^k(N_c-1)(N_c+2)^2(N_c+5)$	0
Δ	N	N	$-\frac{1}{648}I^cS^k(N_c-1)(N_c+2)^2(N_c+5)$	0
Δ	N	Δ	$-\frac{25}{5184}I^cS^k(N_c-1)^2(N_c+5)^2$	$-\frac{5i}{1152}I^c(N_c-1)^2(N_c+5)^2$
Δ	Δ	N	$-\frac{5}{648}I^cS^k(N_c-1)(N_c+2)^2(N_c+5)$	0
Δ	Δ	Δ	$-\frac{1}{648}I^cS^k(N_c-1)(N_c+2)^2(N_c+5)$	$-\frac{i}{288}I^c(N_c-1)(N_c+2)^2(N_c+5)$
Δ	Δ_5	Δ	$-\frac{1}{192}I^cS^k(N_c-3)(N_c-1)(N_c+5)(N_c+7)$	$\frac{i}{128}I^c(N_c-3)(N_c-1)(N_c+5)(N_c+7)$

	$k_{\max}$[MeV]					
Reference	S_{11}	S_{31}	P_{11}	P_{13}	P_{31}	P_{33}
This work	160	200	260	250	260	350
Fettes and Meißner [21]	200	160	200	200	160	170
Torikoshi and Ellis [24]	190	170	220	190	170	220
Yao *et al.* [29]	170	160	170	170	200	240

where the LECs $\alpha_{JI}^{(n)}$ are combinations of those in Eqs. (F41)–(F44).

6. Reductions of spin-flavor operators in the $\pi N \to \pi N$ amplitudes

This appendix provides the reductions of 2-, 3-, and 4-body spin-flavor tensor operators for matrix elements between nucleon states, as needed in the calculation of the $\pi N \to \pi N$ amplitudes. The intermediate state Δ_5 of spin $5/2$ is necessary for the correct general N_c results, and is obviously absent at $N_c = 3$ as shown in the corresponding entries.

APPENDIX G: RANGES OF CONVERGENCE

This appendix compares the results of this work's agreement range with experiment with those of several BChPT studies that include the Δ explicitly in the ϵ expansion, which are most closely related to this work. Reference [21] uses HBChPT, while the others use covariant BChPT with particular regularization schemes. Table VIII shows the approximate maximum CM pion momentum for which the description of phase shifts is consistent. The upper limit of the agreement range is set by the pion momentum above which the data consistently lies outside the bootstrap error band.

[1] J. Gasser, M. E. Sainio, and A. Svarc, Nucleons with chiral loops, Nucl. Phys. **B307**, 779 (1988).
[2] A. Krause, Baryon matrix elements of the vector current in chiral perturbation theory, Helv. Phys. Acta **63**, 3 (1990).
[3] P. J. Ellis and H.-B. Tang, Pion nucleon scattering in a new approach to chiral perturbation theory, Phys. Rev. C **57**, 3356 (1998).
[4] T. Becher and H. Leutwyler, Baryon chiral perturbation theory in manifestly Lorentz invariant form, Eur. Phys. J. C **9**, 643 (1999).
[5] M. R. Schindler, J. Gegelia, and S. Scherer, Infrared regularization of baryon chiral perturbation theory reformulated, Phys. Lett. B **586**, 258 (2004).
[6] C. Hacker, N. Wies, J. Gegelia, and S. Scherer, Including the $\Delta(1232)$ resonance in baryon chiral perturbation theory, Phys. Rev. C **72**, 055203 (2005).
[7] E. E. Jenkins and A. V. Manohar, Baryon chiral perturbation theory using a heavy fermion Lagrangian, Phys. Lett. B **255**, 558 (1991).
[8] E. E. Jenkins and A. V. Manohar, Chiral corrections to the baryon axial currents, Phys. Lett. B **259**, 353 (1991).
[9] E. E. Jenkins and A. V. Manohar, in *Effective Field Theories of the Standard Model*, Proceedings Dobogoko 1991, edited by U.-G. Meißner (World Scientific, Singapore, 1992), p. 113; Report No. UCSD-PTH 91-30, University of California, San Diego.
[10] G. 't Hooft, A planar diagram theory for strong interactions, Nucl. Phys. **B72**, 461 (1974).
[11] J.-L. Gervais and B. Sakita, Large N QCD baryon dynamics: Exact results from its relation to the static strong coupling theory, Phys. Rev. Lett. **52**, 87 (1984).

[12] R. F. Dashen and A. V. Manohar, $1/N_c$ corrections to the baryon axial currents in QCD, Phys. Lett. B **315**, 438 (1993).
[13] G. S. Adkins, C. R. Nappi, and E. Witten, Static properties of nucleons in the Skyrme model, Nucl. Phys. **B228**, 552 (1983).
[14] S. Coleman and J. Mandula, All possible symmetries of the S matrix, Phys. Rev. **159**, 1251 (1967).
[15] E. E. Jenkins, Chiral Lagrangian for baryons in the $1/N_c$ expansion, Phys. Rev. D **53**, 2625 (1996).
[16] A. Calle Cordon and J. L. Goity, Baryon mass splittings in the $1/N_c$ expansion with SU(3) breaking: Effects at arbitrary N_c, Phys. Rev. D **87**, 016019 (2013).
[17] I. P. Fernando and J. L. Goity, Baryon chiral perturbation theory combined with the $1/N_c$ expansion in SU(3): Framework, Phys. Rev. D **97**, 054010 (2018).
[18] M. Mojzis, Elastic πN scattering to $O(p^3)$ in heavy baryon chiral perturbation theory, Eur. Phys. J. C **2**, 181 (1998).
[19] N. Fettes, U.-G. Meißner, and S. Steininger, Pion-nucleon scattering in chiral perturbation theory. Isospin symmetric case, Nucl. Phys. **A640**, 199 (1998).
[20] N. Fettes and U.-G. Meißner, Pion nucleon scattering in chiral perturbation theory. 2.: Fourth order calculation, Nucl. Phys. **A676**, 311 (2000).
[21] N. Fettes and U.-G. Meißner, Pion—nucleon scattering in an effective chiral field theory with explicit spin $3/2$ fields, Nucl. Phys. **A679**, 629 (2001).
[22] N. Fettes and U.-G. Meißner, Complete analysis of pion nucleon scattering in chiral perturbation theory to third order, Nucl. Phys. **A693**, 693 (2001).
[23] T. Becher and H. Leutwyler, Low energy analysis of $\pi N \to \pi N$, J. High Energy Phys. 06 (2001) 017.
[24] K. Torikoshi and P. J. Ellis, Low-energy pion nucleon scattering in the heavy baryon and infrared schemes, Phys. Rev. C **67**, 015208 (2003).
[25] J. M. Alarcon, J. M. Camalich, and J. A. Oller, The chiral representation of the πN scattering amplitude and the pion-nucleon sigma term, Phys. Rev. D **85**, 051503 (2012).
[26] J. M. Alarcon, J. Martin Camalich, and J. A. Oller, Improved description of the πN-scattering phenomenology in covariant baryon chiral perturbation theory, Ann. Phys. (Amsterdam) **336**, 413 (2013).
[27] Y.-H. Chen, D.-L. Yao, and H. Q. Zheng, Analyses of pion-nucleon elastic scattering amplitudes up to $O(p^4)$ in extended-on-mass-shell subtraction scheme, Phys. Rev. D **87**, 054019 (2013).
[28] M. Hoferichter, J. Ruiz de Elvira, B. Kubis, and U.-G. Meißner, Roy–Steiner-equation analysis of pion–nucleon scattering, Phys. Rep. **625**, 1 (2016).
[29] D.-L. Yao, D. Siemens, V. Bernard, E. Epelbaum, A. M. Gasparyan, J. Gegelia, H. Krebs, and U.-G. Meißner, Pion-nucleon scattering in covariant baryon chiral perturbation theory with explicit delta resonances, J. High Energy Phys. 05 (2016) 038.
[30] R. L. Workman, R. A. Arndt, W. J. Briscoe, M. W. Paris, and I. I. Strakovsky, Parameterization dependence of T matrix poles and eigenphases from a fit to πN elastic scattering data, Phys. Rev. C **86**, 035202 (2012).
[31] Data Analysis Center, George Washington University, Institute of Nuclear Studies, https://said.phys.gwu.edu/analysis/pin_analysis.html.
[32] E. Witten, Baryons in the 1/N expansion, Nucl. Phys. **B160**, 57 (1979).
[33] R. F. Dashen and A. V. Manohar, Baryon—pion couplings from large N_c QCD, Phys. Lett. B **315**, 425 (1993).
[34] C. Rosenzweig, J. Schechter, and C. G. Trahern, Is the effective Lagrangian for QCD a sigma model?, Phys. Rev. D **21**, 3388 (1980).
[35] P. Di Vecchia and G. Veneziano, Chiral dynamics in the large N limit, Nucl. Phys. **B171**, 253 (1980).
[36] E. Witten, Large N chiral dynamics, Ann. Phys. (N.Y.) **128**, 363 (1980).
[37] P. Herrera-Siklody, J. I. Latorre, P. Pascual, and J. Taron, Chiral effective Lagrangian in the large N_c limit: The nonet case, Nucl. Phys. **B497**, 345 (1997).
[38] R. Kaiser and H. Leutwyler, Large N_c in chiral perturbation theory, Eur. Phys. J. C **17**, 623 (2000).
[39] R. Flores-Mendieta and C. P. Hofmann, Renormalization of the baryon axial vector current in large-N_c chiral perturbation theory, Phys. Rev. D **74**, 094001 (2006).
[40] H. C. Schroder *et al.*, The pion nucleon scattering lengths from pionic hydrogen and deuterium, Eur. Phys. J. C **21**, 473 (2001).
[41] M. Hennebach *et al.*, Hadronic shift in pionic hydrogen, Eur. Phys. J. A **50**, 190 (2014); **55**, 24(E) (2019).
[42] A. Hirtl *et al.*, Redetermination of the strong-interaction width in pionic hydrogen, Eur. Phys. J. A **57**, 70 (2021).
[43] J. L. Goity and D. Jayakodige (to be published).
[44] S. Navas *et al.* (Particle Data Group), Review of particle physics, Phys. Rev. D **110**, 030001 (2024).
[45] R. F. Dashen, E. E. Jenkins, and A. V. Manohar, The $1/N_c$ expansion for baryons, Phys. Rev. D **49**, 4713 (1994).
[46] R. F. Dashen, E. E. Jenkins, and A. V. Manohar, Spin flavor structure of large N_c baryons, Phys. Rev. D **51**, 3697 (1995).